

Manuscript Number: CERI-D-20-01595R1

Title: Thermal behaviour of vitreous ceramic coatings obtained by electrophoretic deposition for furnace components

Article Type: Full length article

Keywords: Vitreous ceramic coating; Electrophoretic Deposition; Optical properties; Thermal applications

Corresponding Author: Miss Amaia Querejeta,

Corresponding Author's Institution: CIDETEC

First Author: Rosalina Pérez

Order of Authors: Rosalina Pérez; Amaia Querejeta; M. Ángeles Corres; Josemari Muñoz; Hans-Jürgen Grande; Petra Honnerová

Abstract: In this study, three different vitreous ceramic coatings have been designed to improve radiation heat transfer and thereby increase the thermal efficiency of fired heaters or furnaces working at high temperatures. The vitreous ceramic coatings were produced through Electrophoretic Deposition technique (EPD) of ceramic suspensions. These ceramic formulations were designed based on components which increase emissivity, such as SiO<sub>2</sub> and a Black dye (based on chromium, copper and iron oxides), added in 25 wt%. These coatings showed emissivity values around 0.89 at room temperature and around 0.82 at 550 °C in the middle infrared (MIR) spectral range, with slight differences between them. The SiO<sub>2</sub> and Black dye additions provide an important protective effect on the coatings' thermal stability as it was proved by the absorbance level at long times, higher than 85 % in the near infrared (NIR) spectral range. These results were also supported by microstructural characterisation, substrate-coatings adhesion strength and thermal stability tests.

Reviewer #1:  
 Ceramics International  
 Manuscript Number: CERI-D-20-01595

Dear reviewer,

First of all, we would like to thank you for your time and contributions.

We all agree with your comments and suggestions. For this reason author's response is described down below in the following Table:

#	Reviewer's comments	Author's answers:
1	The English must be checked throughout the text.	The English has been checked by our language experts
2	It is not clear why EPD is a "better" technique than other methods to produce such coatings, this must be made more clear in the Introduction	Among all of them, the electrophoretic deposition technique (EPD) is presented as a potential alternative to deposit ceramic coatings onto metallic substrates. This deposition technique has great versatility and significant advantages such as short formation time, simple equipment need, little restriction in substrate complex geometries being able to be easily modified for a specific application (flat, cylindrical or any other shaped substrate with only minor change in the electrode design and positioning), easy control of the thickness and morphology of the deposited film through simple adjustment of the deposition conditions (time and applied potential). The term has been changed in introduction (page 8) and it has been included new reference: D. Vélez, J. Muñoz, J.A. Díez, Influence of application technology in the structural characteristics of ceramic coating with advanced anticorrosive and tribological properties, Adv. Sci. Tech. 91 (2014) 108-116, <a href="https://doi.org/10.4028/www.scientific.net/AST.91.108">https://doi.org/10.4028/www.scientific.net/AST.91.108</a>
3	The rationale behind the selection of the Black dye must be provided more clearly	The selection of a Black dye lies in the fact that a blackbody is an ideal surface, which satisfies three important conditions. First, it is a perfect emitter as it emits more radiant energy than any other surface for a specified temperature and wavelength. Second, a blackbody is the best absorber of energy as it absorbs all energies incident on it from all directions and at all wavelengths. And thirdly, a blackbody is a diffuse emitter as its radiant energy emitted is only a function of temperature and wavelength but is independent of direction. On this basis, the addition of a Black dye will let improve the emissivity results that are pursued in this study.

		The term has been changed in the introduction (page 9) and it has been included a new reference: M. Massoud, Engineering Thermofluids: Thermodynamics, Fluid Mechanics, and Heat Transfer, 2005.
4	<p>a) How were the EPD parameters selected ? By Trial-and-Error"?</p> <p>b) Why were DC and constant voltage conditions used?</p> <p>c) How many samples were coated with one suspension?</p> <p>d) How was the drying process optimised?</p>	<p>a) The EPD parameters were selected after having done an exhausted Design of Experiments study. The reference study is [30] M.R. Pérez García, J. Muñoz, J.A. Díez, Taguchi experimental design method for electrophoretic porcelain enamel (EPE), ECerS 2015 14th International Conference – European Ceramic Society . The term has been changed in Materials and Methods (page 12)</p> <p>b) The use of DC and constant voltage is the recommended way of proceeding as these parameters depend directly on the area to be processed. The amperage increases as a function of the work area and that is the reason why it is a good deposition technique for coating complex geometries.</p> <p>c) 1 sample for each suspension of 100 ml. 6 samples for each formulation has been done for a complete characterisation.</p> <p>d) Later, all the samples were dried in an oven (JP Selecta Digitronic 2005142). The drying conditions were selected through a Design of Experiments study with the aim of achieving a slowly and extended enough process so that the sublimation progress taking place inside the oven does not cause cracks in the ceramic layer during such drying process. As the same of the 4a review, this parameters are selected bases on previous test [30] M.R. Pérez García, J. Muñoz, J.A. Díez, Taguchi experimental design method for electrophoretic porcelain enamel (EPE), ECerS 2015 14th International Conference – European Ceramic Society . The term has been changed in Materials and Methods (page 12)</p>

In addition, you will find the modifications highlighted (in yellow) in the new version of the paper.

February 4<sup>th</sup> of 2020

Dear P. Vincenzini  
General Editor of Ceramics International Editorial

Dear R.K. Bordia  
Editor-in-Chief of Ceramics International Editorial

It is our pleasure to submit the present article entitled: "Thermal behaviour of vitreous ceramic coatings obtained by electrophoretic deposition for furnace components" by **Amaia Querejeta<sup>1</sup>, Rosalina Pérez<sup>1\*</sup>, M<sup>a</sup> Angeles Corres<sup>1</sup>, Josemari Muñoz<sup>1</sup>, Hans-Jürgen Grande<sup>1</sup>, Petra Honnerová<sup>2</sup>**.

<sup>1</sup> CIDETEC, Basque Research and Technology Alliance (BRTA), Po. Miramón 196, 20014 Donostia-San Sebastián, Spain, +34 943 309 022.

[aquerejeta@cidetec.es](mailto:aquerejeta@cidetec.es), [rperez@cidetec.es](mailto:rperez@cidetec.es), [mcorres@cidetec.es](mailto:mcorres@cidetec.es), [jmunoz@cidetec.es](mailto:jmunoz@cidetec.es), [hgrande@cidetec.es](mailto:hgrande@cidetec.es)

<sup>2</sup> Research Centrum - New Technologies, Univerzitni 8, 306 14 Pilsen, Czech Republic. +420 37763 4719

[petrahon@ntc.zcu.cz](mailto:petrahon@ntc.zcu.cz)

Authors of this article **declare that under their ethical responsibility this article is original and unpublished and has not or is not being considered for publication elsewhere**. In addition, all authors declare that **they have seen and approved the manuscript**.

The subject of this paper is the development of high emissivity enamel coatings containing SiO<sub>2</sub> and Black Dye by EPD which have high homogeneity and functional advantages over conventional enamel coatings using other deposition methods. Thermal behavior and high emissivity has been demonstrated using these enamel/SiO<sub>2</sub> and enamel/SiO<sub>2</sub>/Black dye coatings developed.

We would like to request that this paper may please be published in your esteemed journal Ceramics International.

Thank you for your kind consideration and please feel free to contact us for any further information.

Sincerely,



---

Amaia Querejeta Tierno (corresponding author)  
CIDETEC Surface Engineering  
Ceramic Coating Unit  
Donostia - San Sebastian, Spain  
Tel. +34 943 318 212  
[aquerejeta@cidetec.es](mailto:aquerejeta@cidetec.es)

**Declaration of interests**

The authors declare that they have no known competing financial interests or personal relationships that could have appeared to influence the work reported in this paper.

The authors declare the following financial interests/personal relationships which may be considered as potential competing interests:

1 **Thermal behaviour of vitreous ceramic coatings obtained by**  
2  
3  
4 **electrophoretic deposition for furnace components**  
5  
6

7 Rosalina Pérez<sup>a</sup>, Amaia Querejeta<sup>a\*</sup>, M. Ángeles Corres<sup>a</sup>, Josemari Muñoz<sup>a</sup>,  
8  
9  
10 Hans-Jürgen Grande<sup>a</sup>, Petra Honnerová<sup>b</sup>.  
11

12 <sup>a</sup> CIDETEC, Basque Research and Technology Alliance (BRTA), Pº Miramón 196, 20014,  
13  
14 Donostia - San Sebastián, Spain, +34 943 309 022.  
15

16 <sup>b</sup> Research Centre - New Technologies, Univerzitni 8, 306 14 Pilsen, Czech Republic.  
17

18  
19 \*Corresponding author  
20

21 E-mail addresses: [aquerejeta@cidetec.es](mailto:aquerejeta@cidetec.es) (A. Querejeta), [rperez@cidetec.es](mailto:rperez@cidetec.es) (R. Pérez),  
22  
23 [mcorres@cidetec.es](mailto:mcorres@cidetec.es) (M.A. Corres), [jmunoz@cidetec.es](mailto:jmunoz@cidetec.es) (J. Muñoz), [hgrande@cidetec.es](mailto:hgrande@cidetec.es) (H.J.  
24  
25 Grande), [petrahon@ntc.zcu.cz](mailto:petrahon@ntc.zcu.cz) (P. Honnerová)  
26  
27  
28  
29  
30  
31  
32  
33  
34  
35  
36  
37  
38  
39  
40  
41  
42  
43  
44  
45  
46  
47  
48  
49  
50  
51  
52  
53  
54  
55  
56  
57  
58  
59  
60  
61  
62  
63  
64  
65

1                   **Abstract**  
2  
3

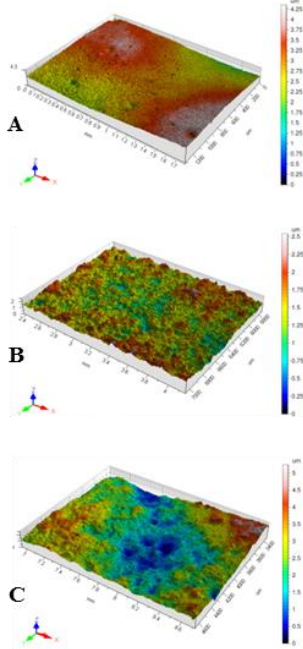
4                   In this study, three different vitreous ceramic coatings have been designed to improve  
5 radiation heat transfer and thereby increase the thermal efficiency of fired heaters or  
6 furnaces working at high temperatures. The vitreous ceramic coatings were produced  
7 through Electrophoretic Deposition technique (EPD) of ceramic suspensions. These  
8 ceramic formulations were designed based on components which increase emissivity,  
9 such as SiO<sub>2</sub> and a Black dye (based on chromium, copper and iron oxides), added in 25  
10 wt%. These coatings showed emissivity values around 0.89 at room temperature and  
11 around 0.82 at 550 °C in the middle infrared (MIR) spectral range, with slight  
12 differences between them. The SiO<sub>2</sub> and Black dye additions provide an important  
13 protective effect on the coatings' thermal stability as it was proved by the absorbance  
14 level at long times, higher than 85 % in the near infrared (NIR) spectral range. These  
15 results were also supported by microstructural characterisation, substrate-coatings  
16 adhesion strength and thermal stability tests.  
17  
18  
19  
20  
21  
22  
23  
24  
25  
26  
27  
28  
29  
30  
31  
32  
33  
34  
35  
36  
37  
38  
39  
40  
41  
42  
43  
44  
45  
46  
47  
48  
49  
50  
51  
52  
53  
54  
55  
56  
57  
58  
59  
60  
61  
62  
63  
64  
65

1 **Keywords:** Vitreous ceramic coating; Electrophoretic Deposition; Optical properties;  
2  
3  
4 Thermal applications  
5  
6  
7  
8  
9  
10  
11  
12  
13  
14  
15  
16  
17  
18  
19  
20  
21  
22  
23  
24  
25  
26  
27  
28  
29  
30  
31  
32  
33  
34  
35  
36  
37  
38  
39  
40  
41  
42  
43  
44  
45  
46  
47  
48  
49  
50  
51  
52  
53  
54  
55  
56  
57  
58  
59  
60  
61  
62  
63  
64  
65

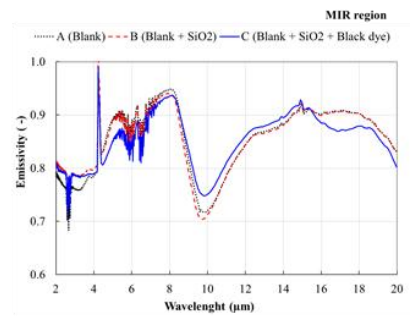
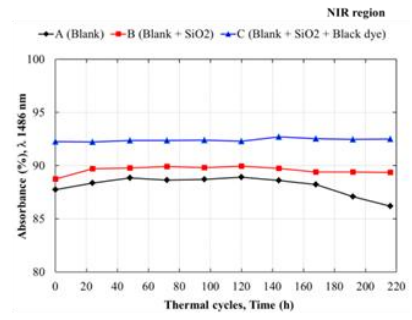
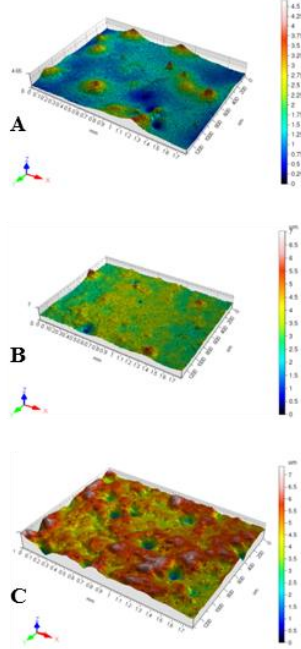


# Graphical Abstract

Before thermal stability



After thermal stability



1           **Highlights**  
2  
3

- 4           • Homogeneous vitreous ceramic coatings containing 25 wt% SiO<sub>2</sub> and 25 wt%.  
5           Black dye were obtained by electrophoretic deposition.  
6  
7
- 8           • Ceramic coatings exhibited normal emissivity values around 0.89 at room  
9           temperature and around 0.82 at 550 °C in the MIR range.  
10
- 11          • Ceramic coatings maintained an absorbance level around 85 % in the NIR range  
12          after 216 h at 550 °C.  
13
- 14          • SiO<sub>2</sub> and Black dye provide thermal stability to ceramic coatings at 550 °C after  
15          long thermal cycles.  
16  
17  
18  
19  
20  
21  
22  
23  
24  
25  
26  
27  
28  
29  
30  
31  
32  
33  
34  
35  
36  
37  
38  
39  
40  
41  
42  
43  
44  
45  
46  
47  
48  
49  
50  
51  
52  
53  
54  
55  
56  
57  
58  
59  
60  
61  
62  
63  
64  
65

## 1. Introduction

Western Europe is nowadays facing an increasingly growing shortage of energy resources. Raw materials, especially those from the petrochemical sector, have more limited availability and, therefore, their prices show a growing trend. The price of energy from these sources has already become one of the main fixed operating costs in the industry and an exponential increase is expected in the short-medium term. That is why, increased energy efficiency has been established as a key objective (i.e. the European Commission's target is to increase energy efficiency up to 32.5% by 2030 [1] prioritizing a better use of existing energy).

With this in mind, among the different productive processes there are industries using fired heaters or furnaces whose concern is to maximise the efficiency of boilers with the aim of reducing fuel consumption. This versatile heat transfer equipment is very common in numerous industries such as refineries, petrochemicals, production of ceramics, glass and steel [2]. For instance, the iron and steel industry are one of the most energy consuming manufactures since energy is consumed during several stages of the production process: raw materials preparation, casting, finishing, heat treatment, to mention just a few.

Furnaces are also used in reheating processes [3] to heat steel shapes in order to get a suitable plastic deformation in the rolling stage. They are continuous processes which occur in a furnace where the stock is a charged, heated and discharged while producing energy transfers by means of convection and radiation from the hot burner gases and the furnace walls [4]. As a result of the high temperature of the combustion gases and the furnace walls, most of the heat transfer is carried out by radiation, and subsequently, any small improvement in thermal efficiency significantly increases the production

1 yields and even reduces consumption of fuel [4]. Radiance emitted from the surface  
2  
3 principally depends on two factors: a) the surface temperature, which is an indication of  
4  
5 the equilibrium thermodynamic state resulting from the energy balance of the fluxes  
6  
7 between the grey body surface and its surroundings; and b) the surface emissivity,  
8  
9 which is the efficiency of transmission of radiant energy generated in the surface into its  
10  
11 surroundings. The surface emissivity, in turn, depends on the temperature, the nature of  
12  
13 the material (its composition), the surface parameters (roughness, thickness, etc.) and  
14  
15 the wavelength. In general, solid materials always emit energy over the entire  
16  
17 wavelength spectrum but for a non-grey surface, the emissivity is a value that depends  
18  
19 on the wavelength [2,5,6]. It has been previously established that most polar bonding  
20  
21 oxides show strong efficiency of photon emission thus exhibiting a high emissivity  
22  
23 value [7].  
24  
25  
26  
27  
28

29  
30 90 % of the heat energy transferred in furnaces with operational temperature 700 to  
31  
32 1200 °C is produced in the Near IR band spectral zone, between 1.5 and 6.4  $\mu\text{m}$  [2,8].  
33  
34

35 In this respect, the application of high emissivity coatings [2,4,7,9,10,11] in these  
36  
37 furnace components improves heat transfer considerably while producing important  
38  
39 energy savings without compromising process reliability, operation safety, and  
40  
41 ultimately increasing thermal efficiency. Over the last years, major development and  
42  
43 research effort have been carried out to analyse the benefits and advantages of high-  
44  
45 emissivity coatings in order to substantially improve their performance [2]. These  
46  
47 coatings mainly consist of materials capable of absorbing and re-radiating thermal  
48  
49 energy such as SiC, Si<sub>3</sub>N<sub>4</sub> and Al<sub>2</sub>O<sub>3</sub> [12,13]; Zr-B<sub>2</sub>-SiC [14]; or SiC/SiO<sub>2</sub> [15].  
50  
51

52 However, at the same time, they are coatings designed to perform other important tasks:  
53  
54 good adhesion strength, high resistance to abrasion, good resistance to thermal shock,  
55  
56  
57  
58  
59  
60  
61  
62  
63  
64  
65

1 thermal expansion coefficient similar to metal substrates to prevent surface defects [2]  
2  
3 to name a few.  
4

5  
6 The definition describes emissivity as the ratio of the thermal radiation from ideal black  
7  
8 surface (classified with an emissivity value of 1) at the same temperature given by the  
9  
10 Stefan-Boltzmann law; it is also possible to obtain high emissivity surfaces by  
11  
12 developing black surfaces [16,17].  
13  
14

15  
16 In summary, high emissivity coatings capable of maximising and stabilising surface  
17  
18 emissivity over various thermal processes, delivering as a consequence quick and  
19  
20 efficient heat transfer, uniform heating and even a longer service life [18,19,20].  
21

22  
23 Many techniques for the production of ceramic coatings have been proposed, such as  
24  
25 conduction and diffusion processes (electrostatic deposition, electrophoretic coating,  
26  
27 electrolytic deposition...), chemical processes (chemical vapour deposition, plasma...),  
28  
29 wetting processes (dip coating, spin coating...), spraying processes (flame spray,  
30  
31 detonation spray...) and physical vapour deposition processes (sputter deposition, ion  
32  
33 beam deposition...) [21]. Among all of them, the electrophoretic deposition technique  
34  
35 (EPD) is presented as a potential alternative to the deposition of ceramic coatings onto  
36  
37 metallic substrates. This deposition technique offers great versatility and significant  
38  
39 advantages such as short formation time, only simple equipment needed, reduced  
40  
41 coating costs, little restriction in substrate complex geometries which can be easily  
42  
43 modified for a specific application (flat, cylindrical or any other shaped substrate with  
44  
45 only minor change in the electrode design and positioning), easy control of the thickness  
46  
47 and morphology of deposited films through simple adjustment of the deposition  
48  
49 conditions (time and applied potential), excellent edge coverage...The EPD technique  
50  
51 lets deposit ceramic coatings on complex geometry substrates, lets control the layer  
52  
53  
54  
55  
56  
57  
58  
59  
60  
61  
62  
63  
64  
65

1 thickness and morphology in short deposition times using a simple EPD equipment

2  
3 [22,23,24,25]. The EPD principle is based on subjecting a stable colloidal suspension in  
4  
5 a liquid medium to an electric field between two electrodes so that the charged particles  
6  
7 are attracted to and deposited onto the conductive substrate. The process has to be  
8  
9 regulated to achieve a homogeneous ceramic layer by stabilizing the suspension  
10  
11 (particle size distribution, pH, conductivity, viscosity...) and the electrical conditions  
12  
13 (deposition time and applied voltage) [22].  
14  
15  
16

17  
18 Considering the ease of the deposition technique, it has been selected a good option to  
19  
20 properly design high emissivity ceramic coatings that could apply layers on metallic  
21  
22 components placed inside furnaces. Three different ceramic formulations have been  
23  
24 designed using components which increase the coatings' emissivity such as SiO<sub>2</sub> and a  
25  
26 Black dye (considering its black nature and the presence of oxides in its composition  
27  
28 which provide excellent chemical stability) [26], with the aim of obtaining surfaces with  
29  
30 great advantages in heat transfer, delivering higher energy efficiency in purpose-built  
31  
32 industrial processes. These emissivity results were also supported by adhesion strength,  
33  
34 thermal stability, and microstructural tests.  
35  
36  
37  
38  
39

40 The selection of a Black dye lies in the fact that a blackbody is an ideal surface, which  
41  
42 meets three important conditions. First, it is a perfect emitter as it emits more radiant  
43  
44 energy than any other surface for a specified temperature and wavelength. Second, a  
45  
46 blackbody is the best absorber of energy as it absorbs all energies approaching it from  
47  
48 all directions and at all wavelengths. Thirdly, a blackbody is a diffuse emitter since its  
49  
50 radiant energy emitted is only a function of temperature and wavelength, yet  
51  
52 independent of direction [27]. Taking the above into account, the addition of a Black  
53  
54 dye will improve the emissivity results that are pursued in this study.  
55  
56  
57  
58  
59  
60  
61  
62  
63  
64  
65

## 2. Materials and Methods

Commercial frit VP15/1546 (supplied by Prince Minerals) was used as main raw material which set the ceramic matrix to obtain the vitreous ceramic coatings. This frit, based on inorganic elements ( $\text{SiO}_2$ ,  $\text{Al}_2\text{O}_3$ ,  $\text{Na}_2\text{O}$ ,  $\text{CaO}$ ,  $\text{CoO}$  and  $\text{TiO}_2$ ) [28] which provide good chemical resistance, is widely used in coated heat exchangers.

### 2.1. Preparation of ceramic suspensions

The ceramic suspensions were prepared by mixing the frit with refractory materials, additives and setting agents in order to obtain three different formulations:

- A (Blank): the frit was ball-milled (MGS Rulli 1P supplied by Heramika S.L.) for 3 h with the addition of 4 wt% clay ( $\text{Al}_2\text{O}_3 \cdot \text{SiO}_2 \cdot \text{H}_2\text{O}$ ), 0.5 wt% bentonite, 0.15 wt% carboxymethyl cellulose and 70 wt% distilled water. With the aim of obtaining an optimum milling process, the percentage of solids,  $\text{Al}_2\text{O}_3$  balls and free space was balanced in volume by mixing a mass of 150 g of solid, with the above-mentioned composition with 70 mL of distilled water and 160 mL of  $\text{Al}_2\text{O}_3$  balls. This formulation served as reference.
- B (Blank +  $\text{SiO}_2$ ): it is based on formulation A but with the addition of 25 wt% of quartz  $\text{SiO}_2$  (Prince Minerals commercial powder).
- C (Blank +  $\text{SiO}_2$  + Black dye): it is based on formulation A but with the addition of 25 wt% of quartz  $\text{SiO}_2$  (Prince Minerals commercial powder) and 25 wt% of Black dye (Prince Minerals commercial powder based on Cr, Cu, Fe oxides). The composition of the Black dye, characterised by SEM-EDX,

1 consist of  $46.60 \pm 0.95$  of O,  $26.97 \pm 0.67$  of Cr,  $15.33 \pm 0.78$  of Cu, and  
2  
3  
4  $11.10 \pm 0.52$  of Fe (values expressed in wt%).

5  
6 After the milling process, the three slurries were controlled in terms of density ( $1.60$   
7  $\text{g/cm}^3$ ) and viscosity (120 s flowing time in Ford cup no. 2). A sieve was used so that it  
8  
9 would be possible to test the grain size a  $44 \mu\text{m}$  (aperture:  $16,900 \text{ mesh/cm}^2$ ), and the  
10  
11 absence of any solid residual above this size was checked in accordance with ISO  
12  
13 3310/1:2016 [29].  
14  
15

16  
17 The initial pH value was approximately 11 in each formulation. 3 ml of sodium  
18  
19 aluminate 43 % (ALNA<sup>®</sup> 73, IQE group) per each 100 g of frit was added to obtain a  
20  
21 final conductivity of  $3.11 \text{ mS/cm}$  and a pH of 13, which was further decreased to 12 by  
22  
23 adding HCl 1N (1 mol/solution, Scharlau). Eventually, 0.1 % sodium dodecyl sulphate  
24  
25 (SDS) anionic surfactant was added to achieve colloidal stability of the slurry.  
26  
27  
28  
29  
30

## 31 *2.2. Preparation of ceramic coatings: EPD process*

32  
33  
34

35 Ceramic coatings were deposited onto metallic substrate by the electrophoretic  
36  
37 deposition technique (EPD). Square plates of 310 stainless steel were used as substrate  
38  
39 ( $50 \text{ mm} \times 50 \text{ mm} \times 1 \text{ mm}$ ), which were pre-treated by sandblasting in a Norblast FN -  
40  
41 30T grit-blasting equipment operated with white corundum GR100, Coniex. This  
42  
43 previous step allowed the removal of surface impurities as well as provided a specific  
44  
45 suitable surface area. Subsequently, the substrates were cleaned with deionized water  
46  
47 and compressed air prior to the EPD process. In the EPD, based in a two-electrode cell,  
48  
49 the cleaned substrates to be deposited acted as the positive electrode (anode), while  
50  
51 another stainless steel plate with similar dimensions acted as the negative electrode  
52  
53 (cathode). Both plates were placed into a glass baker containing the ceramic suspension  
54  
55  
56  
57  
58  
59  
60  
61  
62  
63  
64  
65



1 (100 mL), at a distance of 20 mm. Deposition occurs when the suspended ceramic  
2  
3 particles adhere to the work piece under an electric field forming a foam-structured  
4  
5 solid layer while electro-osmotic dewatering takes place.  
6  
7

8 All EPD experiments (three formulations: A, B, C) were carried out at room  
9  
10 temperature by applying a constant voltage of 20 V using a DC power supply  
11  
12 (Blausonic FA-350), with a deposition time of 20 s, as established after a Design of  
13  
14 Experiments study [30]. The study, based on a Taguchi experimental design, allows  
15  
16 obtaining a desirable thickness in the ceramic coating under various conditions  
17  
18 developed by EPD. An orthogonal array of  $L_{16}(2^{15})$  type at two levels of control factors  
19  
20 was utilised to determine the significant factors affecting the deposition rate. The 15  
21  
22 factors studied were divided in four basic stages of the EPD process: substrate  
23  
24 (including substrate and pre-treatment), formulation (including concentration, pH,  
25  
26 density and particle size), EPD system (including applied voltage, exposure area,  
27  
28 deposition time, distance between electrodes, systems temperature and rinsed off) and  
29  
30 heat treatment (including drying temperature, drying time, sintering temperature and  
31  
32 sintering time). After the deposition processes, the obtained samples were first rinsed  
33  
34 out with deionized water to remove all excess non-charged particles and to obtain a  
35  
36 smooth surface finish.  
37  
38

39  
40  
41  
42  
43  
44 Subsequently, all the samples were dried in an oven (JP Selecta Digitronic 2005142).  
45  
46  
47 The drying conditions were selected through a Design of Experiments study with the  
48  
49 aim of achieving a slow, sufficiently extended process so that the sublimation inside the  
50  
51 oven does not develop cracks in the ceramic layer during the drying process.  
52  
53

54 The sintering process of the coated samples was carried out in air atmosphere using a  
55  
56 Hobersal HD230-PAD furnace, in order to consolidate the ceramic coating and boost its  
57  
58

1 adhesion strength to the substrate. The sintering temperature of the different dried  
2  
3 formulations was determined on the basis of the melting point obtained by heating  
4  
5 microscopy (Expert System Misura HSML ODLT 1400- 30) from 500 °C to 1200 °C at  
6  
7 a 1 °C/min heating rate (Table 1). Thus, Samples A, B and C were sintered at 780, 827  
8  
9 and 914 °C, respectively.  
10  
11  
12  
13

### 14 *2.3. Characterisation of experiments*

15  
16  
17

18 Distribution of the particle sizes of the ceramic formulations was analysed using a  
19  
20 Mastersizer 3000 MAZ 6140 supplied by MALVERN Instruments Ltd, to determine  
21  
22 DV(10), DV(50) and DV(90) parameters which represent the maximum particle  
23  
24 diameter below 10 %, 50 % and 90 % of the samples volume respectively.  
25  
26

27 Evaluation of sintering behaviour of the dried powder formulations was performed  
28  
29 using a heating microscope (Expert System Misura HSML ODLT 1400-30) over a wide  
30  
31 temperature range, from 500 °C to 1200 °C at a 1 °C/min heating rate (Table 1) with a  
32  
33 temperature accuracy of 0.1 °C. This characterisation technique provides useful  
34  
35 information to establish the optimum firing conditions, which let consolidate the  
36  
37 coatings to the metallic substrate. For this purpose, dried ceramic powder was shaped in  
38  
39 small cylinders with a height of 3 mm and a diameter of 1 mm and placed over alumina  
40  
41 slabs inside the furnace of the heating microscope for testing. The software, which  
42  
43 combines thermal treatment with image analysis, provides five characteristic  
44  
45 temperatures: a) the first shrinkage with a 5 % dimensional change ( $T_{\text{sintering}}$ ); b) the  
46  
47 maximum shrinkage where rounded edges and smooth walls appear ( $T_{\text{softening}}$ ); c) the  
48  
49 ball point where the first signal of melting appears and the sample looks like a perfect  
50  
51 theoretic sphere ( $T_{\text{sphere}}$ ); d) the half ball point where the sample height is half its base  
52  
53  
54  
55  
56  
57  
58  
59  
60  
61  
62  
63  
64  
65

1 (T<sub>half sphere</sub>); and e) the flow point where the sample collapses to a third of its height at  
2  
3 the hemisphere state (T<sub>melting</sub>) (following DIN 51730 standard) [31]. Thus, the melting  
4  
5 temperatures obtained by heating microscopy were the ones used as sintering  
6  
7 temperature of the different dried formulations.  
8  
9

10 The adherence test was performed using an impact tester (supplied by Neurtek) in  
11  
12 accordance with UNE-EN-10209 standard [32] where the adherence strength of the  
13  
14 ceramic coating is measured after a ball impact that generates a deformation in the  
15  
16 substrate. In this experimental setup, a load of 1.5 kg steel ball is applied from a specific  
17  
18 height depending on the steel sheet thickness, 750 mm for this case corresponding to  
19  
20 1.2-3 mm steel sheet thickness. The adherence intensity between the ceramic coating  
21  
22 and metal substrate was assessed according to the remnants of vitreous ceramic coating  
23  
24 on the destroyed surface. Accordingly, the strength of coating adherence is classified by  
25  
26 visual inspection into grades from 1 to 5, with 1 being the best (if most of the ceramic  
27  
28 layer remains on the steel sheet) and 5 the worst (if most of the ceramic layer is  
29  
30 removed from the steel sheet, and the surface appears silvery bright).  
31  
32  
33  
34  
35  
36

37 Thermal stability tests were carried out by cyclic heating up to 550 °C for 24 h and then  
38  
39 cooling down to room temperature, reaching 216 h in total. The surfaces of the samples  
40  
41 were evaluated every 24 h focusing on their optical properties and appearance.  
42  
43  
44

45 A Nikon SMZ800N microscope was used to obtain high-resolution images of minute  
46  
47 surface structures at 16.3x magnifications.  
48

49 A scanning electron microscopy (SEM JEOL JSM 5500 LV) equipped with energy-  
50  
51 dispersive X-ray (EDX) microanalysis systems (INCAx-sight 6617, Oxford Instruments  
52  
53 Analytical, England) was used to characterise the microstructure of the deposited films.  
54  
55  
56

57 Coating thickness was calculated as an average of three measurements taken from  
58  
59  
60  
61  
62  
63  
64  
65

1 micrographs at 100x magnification. All the samples were sputtered with gold prior to  
2  
3 SEM-EDX analyses. Microanalyses were performed using an electron beam  
4  
5 acceleration voltage of 20 kV and an acquisition time of 5 minutes. The superficial and  
6  
7 cross-sectional EDX analyses and mapping were performed to evaluate the distribution  
8  
9 of chemical elements, such as Si, Fe, Cr and Cu, in the ceramic coatings.  
10

11  
12 Topographical maps of the surfaces of ceramic coatings were acquired using a confocal  
13  
14 microscope (Leica Microsystems, DCM 3D), which employs a blue light source ( $\lambda=470$   
15  
16 nm) for better resolution, with objective magnification of 20x and 50x for high  
17  
18 resolution images analysed by LeicaMap software (Leica Microsystems). Each sample  
19  
20 was scanned over three areas of approximately 1.5 x 1.5 mm size.  
21  
22

23  
24 Absorbance and emissivity were analysed at room temperature. Absorbance  
25  
26 measurements were acquired in a JASCO V-570 UV-VIS-NIR Spectrophotometer fitted  
27  
28 with a double-beam system with a single monochromator in the wavelength range  
29  
30 between 280 and 2500 nm, with 0.5 nm resolution, and equipped with a JASCO ILN-  
31  
32 472 Integrating Sphere of 15 cm diameter for diffuse reflectance and transmittance. This  
33  
34 spectrophotometer was used to measure spectral normal reflectance.  
35  
36  
37

38  
39 An indirect emissivity measurement method [33] was used for analysis of samples at  
40  
41 room temperature (25°C). Spectral normal hemispherical reflectance was measured by a  
42  
43 Nicolet 6700 FTIR spectrometer equipped with a IntegratIR<sup>TM</sup> commercial integrating  
44  
45 sphere system from PIKE Technologies with an incidence angle of 12° in the spectral  
46  
47 range from 2 to 20  $\mu\text{m}$ .  
48  
49

50  
51 The measured values of reflectance were used for calculation of spectral normal  
52  
53 absorbance and emissivity, assuming the total transmittance as zero for opaque surfaces  
54  
55 according to Kirchhoff's law [34].  
56  
57  
58  
59  
60  
61  
62  
63  
64  
65

1 For emissivity analysis of samples at high temperature, a direct emissivity measurement  
2  
3 method was used [35]. The method is based on a comparison of black body and sample  
4  
5 radiation at the same temperature, under the same spectral and geometric conditions.  
6  
7

8 The exact temperature of the sample surface was determined using a FLIR A320  
9  
10 infrared camera and a reference coating with a known effective emissivity applied on  
11  
12 one half of each sample. By this method, spectral normal emissivity was analysed at a  
13  
14 temperature of 550°C in the spectral range from 2 to 26  $\mu\text{m}$ .  
15  
16  
17

18 Band normal emissivity with the weight of radiation intensity at the sample radiation  
19  
20 temperature according to Planck's law [36] was calculated from spectral quantities. The  
21  
22 band from 5 to 20  $\mu\text{m}$  was selected for room temperature and the band from 2 to 9  $\mu\text{m}$   
23  
24 was selected for the sample temperature of 550 °C. In these spectral zones, over 75 % of  
25  
26 the heat energy is transferred for examined temperatures.  
27  
28  
29  
30  
31  
32  
33  
34  
35  
36  
37  
38  
39  
40  
41  
42  
43  
44  
45  
46  
47  
48  
49  
50  
51  
52  
53  
54  
55  
56  
57  
58  
59  
60  
61  
62  
63  
64  
65

1       **3. Results and Discussion**  
2  
3

4               *3.1. Characterisation of ceramic formulations*  
5  
6

7                       *3.1.1. Particle size distribution*  
8  
9

10  
11       The ceramic formulations have a particle size distribution slightly changed by the  
12       addition of SiO<sub>2</sub> and Black dye. As shown in Figure 1, the blank formulation, without  
13       any additions, has a multimodal distribution (black line) with a mean DV(90) of around  
14       46 µm but with four outstanding maximums (0.9, 3.0, 20.0, and 180 µm). When this  
15       blank formulation is mixed with SiO<sub>2</sub> (red line), the mean DV(90) is barely modified to  
16       higher values with two outlined maximums (0.9 and 15.0 µm), achieving a more  
17       homogeneous distribution. The addition of the Black dye (blue line) reduces more  
18       notably the mean DV(90) value to approximately 38 µm generating one main defined  
19       maximum, delivering the most homogeneous size distribution. In any case, the three  
20       ceramic formulations have a suitable and homogeneous particle size distribution [37] to  
21       be applied by the EPD technique.  
22  
23  
24  
25  
26  
27  
28  
29  
30  
31  
32  
33  
34  
35  
36  
37  
38

39                       *3.1.2. Sintering and melting behaviour*  
40  
41

42       The evaluation of sintering and melting behaviour allows establishing the characteristic  
43       temperatures of the three dried powder formulations (Table 1). In these data, the melting  
44       temperature is the most important parameter in the firing process, as the ceramic  
45       formulation is completely fluidized, thus enabling the reaction gases to exit and  
46       strengthening the chemical bond with the metallic substrate.  
47  
48  
49

50       Clays, silica and set-up salts are inorganic components added to the slip to adjust the  
51       rheological parameters and stabilize the suspension. Some of the components are  
52  
53  
54  
55  
56  
57  
58  
59  
60  
61  
62  
63  
64  
65

1 refractories, such as silica and, as a result, more resistant to firing process that can be  
2  
3 checked by the increase in the characteristic temperatures. In general, a temperature  
4  
5 increase is shown with the additions, a more pronounced increase for Sample C which is  
6  
7 seen in the whole temperature range compared to Sample B which is only noticeable in  
8  
9 the  $T_{\text{sphere}}$ ,  $T_{\text{half sphere}}$  and  $T_{\text{melting}}$ . This behaviour is due to the greater refractory character  
10  
11 of the Sample C. Therefore, the  $\text{SiO}_2$  addition (Sample B) transposes these temperatures  
12  
13 to upper ranges (more than 40 °C in the melting temperature), as  $\text{SiO}_2$  is a thermally  
14  
15 stable component to high temperatures. On the other hand, the addition of metallic  
16  
17 oxides present in the Black dye composition also improves the sintering and melting  
18  
19 behaviour, as metallic oxides are known to prepare pigments resistant to extreme  
20  
21 working conditions because of their excellent chemical stability [26]. In this case, the  
22  
23 Black dye is based on Fe, Cr and Cu oxides, which are metallic oxides with high  
24  
25 melting points; they do increase the characteristic temperatures by more than 130 °C in  
26  
27 the melting temperature.  
28  
29  
30  
31  
32  
33

### 36 *3.2. Characterisation of ceramic formulations*

#### 39 *3.2.1. Adherence strength test*

42  
43 The degree of adherence has been assessed by an impact test according to UNE-EN-  
44  
45 10209 standard [32]. The results of the three samples show that most of the ceramic  
46  
47 layer remaining on the steel sheet (Figure 2) generated an excellent adherence strength  
48  
49 of Grade 1 (defined as the impact surface being completely covered by ceramic coating  
50  
51 although the coating is broken, and metallic substrate is not appreciated) on a 1 to 5  
52  
53 grade scale (where Grade 5 defined as an impact surface showing a complete  
54  
55 delamination of the ceramic coating-substrate interface). This is supported by true  
56  
57  
58  
59  
60  
61  
62  
63  
64  
65

1 images where no significant changes can be detected after the addition of SiO<sub>2</sub> and  
2  
3 Black dye.  
4

5  
6 The excellent adherence strength of coatings is caused by the formation of dendritic  
7  
8 structures established between the steel and the vitreous ceramic coating [38,39,40]. The  
9  
10 firing process ensures the consolidation of the ceramic coating to the metallic substrate  
11  
12 by a chemical bonding, thanks to several complex chemical reactions taking place in the  
13  
14 interface. During the heating process of the initial stage, metallic substrate surface  
15  
16 undergoes oxidation processes which create a thin oxide layer that is entirely dissolved  
17  
18 by the molten ceramic coating at temperatures above 600 °C. As a result, iron oxides  
19  
20 penetrate into the ceramic layer and cobalt ions are simultaneously reduced at the metal-  
21  
22 ceramic phase boundary to dendritic crystals of metallic cobalt, they alloy with iron and  
23  
24 promote the oxidation of the base metal [41]. As a consequence, the metallic surface  
25  
26 increases its roughness generating many mechanical anchor points to which the ceramic  
27  
28 coating can adhere [42,43].  
29  
30  
31  
32  
33

34  
35 A reaction scheme of the chemical processes taking place during thermal treatment is  
36  
37 shown in Table 2. According to the scheme, the chemical bond between the steel and  
38  
39 the ceramic coating mainly depends on the concentration of cobalt in the coating, the  
40  
41 redox condition at the metal-ceramic coating phase boundary is strongly influenced by  
42  
43 the carbon dioxide release from steel and the partial pressure of oxygen and thermal  
44  
45 treatment parameters such as time and temperature [44,45]. This chemical bond is  
46  
47 responsible for the strong adherence between the ceramic coating and the steel  
48  
49  
50  
51  
52 substrate.  
53  
54  
55  
56  
57  
58  
59  
60  
61  
62  
63  
64  
65



### 3.2.2. Thermal Stability

Thermal stability of vitreous coatings was evaluated according to the behaviour of the coatings before and after the thermal load. Visual changes at microscopic and macroscopic level along with changes in the roughness and thickness of the coatings provide basic information about thermal stability of the coatings. The microstructure of ceramic coating, especially the distribution of porosity and bubbles, the elemental composition of coatings and SiO<sub>2</sub> content on surface of coatings give more detailed information.

Images analysis on both a macroscopic and microscopic level was performed over the cycles of thermal stability test (Table 3) for the three ceramic coatings. Minor changes in the colour tone are observed at macroscopic level while in a greater detail, at microscopic level, a bigger loss of tone is shown. This indicates that the samples have undergone a certain visual degradation that may have been caused by the increased roughness of the coating after thermal load.

Three different morphologies are shown by 3D mapping (Table 4). In general, with the increased addition of SiO<sub>2</sub> and Black dye, the surface roughness (Ra) increases (Table 5) by approximately 10 % for Samples B and C in comparison to Sample A.

On the other hand, it has been seen that thermal stability test promotes higher surface roughness in all cases; this holds especially for Sample A in terms of the initial morphology that increases by one order of magnitude. As expected, the additions, both SiO<sub>2</sub> and Black dye, increase the initial roughness and the increment appears sharper for Sample C as a consequence of having the two additions in the same coating. After the thermal stability test, both Sample B and C experience an increase in roughness, which

1 is more pronounced in the sample having SiO<sub>2</sub> and Black dye additions as there are  
2  
3 more components not embedded in the vitreous net.  
4

5  
6 Output data from the SEM-EDX characterisation is used for identification and  
7  
8 distribution of certain inorganic elements present in the ceramic coatings via the  
9  
10 mapping analysis and their semi-quantitative determination. The three ceramic coatings  
11  
12 show a homogeneous distribution of silicon, iron, chromium and copper (Table 6).  
13  
14

15  
16 The silicon content (the green points homogeneously distributed throughout the coating  
17  
18 layer) is present in the three formulations; however, it must be noted that Sample A  
19  
20 shows Si content as a consequence of the element being present in the frit composition,  
21  
22 as explained in detail above in Section 2. The Fe content is prevalent in the interface as  
23  
24 a result of chemical bonding between the vitreous ceramic coating and the steel  
25  
26 substrate. Furthermore, a certain level of Fe has also been recorded throughout the layer  
27  
28 of the coating (blue points) for Sample C due to the addition of Black dye, which is  
29  
30 based on Cr, Cu, Fe. In this situation, chromium acts as iron because it also has a role in  
31  
32 the chemical bonding. Chromium comes from the steel substrate and takes part in the  
33  
34 redox reactions and therefore appears in the Black dye composition (purple points).  
35  
36 Copper is subtly present both in the ceramic coating (Sample A and B); its levels are  
37  
38 higher in Sample C due to the composition of the Black dye (pink points).  
39  
40  
41  
42  
43

44  
45 The SEM-EDX mappings taken after the thermal stability tests follow the same trend,  
46  
47 supporting the idea of coatings being thermally stable.  
48

49  
50 Furthermore, the ceramic coating microstructure provides very valuable information to  
51  
52 predict the final properties of the coating. In this sense, the porosity and bubbles  
53  
54 formation do play an important part. Porosity is the result of gas formation during the  
55  
56 heating process as a consequence of the high temperature chemical reactions taking  
57  
58  
59  
60  
61  
62  
63  
64  
65

1 place between the metallic substrate and the ceramic coating. Indeed, the generated  
2  
3 gases are N<sub>2</sub>, CO<sub>2</sub>, water vapour, H<sub>2</sub> and CH<sub>4</sub> [46,47]. In the specific case of water  
4  
5 vapour, this is formed at about 500 °C when the clay, a component of the ceramic  
6  
7 formulation, decomposes. Part of this steam is remains trapped as fine bubbles in the  
8  
9 continuous vitreous ceramic layer once the melting ceramic coating cools. This  
10  
11 microstructure is known as bubble structure or close porosity. It is a typical feature of  
12  
13 the ceramic coating and the phenomenon responsible for providing flexibility to  
14  
15 vitreous coating. In the formation process of this microstructure [38], the size and  
16  
17 distribution of the bubbles are important; they highly depend on the conditions of the  
18  
19 thermal treatment, on viscosity of ceramic coating, and on surface tension [47].  
20  
21 Therefore, small bubbles present in under-fired ceramic coatings have very poor  
22  
23 adherence strength while over-fired coatings form bubbles of too large size or either no  
24  
25 bubble structure at all. In result, the coating becomes very brittle and prone to cracking  
26  
27 under low impact or stress. When the ceramic coating is subjected to the optimum firing  
28  
29 process, its microstructure is based on a structure of medium-size bubbles  
30  
31 homogeneously distributed.  
32  
33 In this study, SEM micrographs (Table 7) show some differences in bubble structure  
34  
35 between samples but it is evident that the bubbles are not interconnected in any of the  
36  
37 cases and remain confined in the coating layer, thus guaranteeing good protection of the  
38  
39 metallic substrate against corrosion [45]. Quite homogeneous distribution of two types  
40  
41 of bubble size all along the coating thickness (see Table 6) could be seen from the  
42  
43 ceramic coating micrograph without additions (Sample A).  
44  
45 The addition of 25 % quartz to the ceramic formulation (Sample B) causes a reduction  
46  
47 in the quantity of small and large bubbles, and generates SiO<sub>2</sub> aggregates (black  
48  
49  
50  
51  
52  
53  
54  
55  
56  
57  
58  
59  
60  
61  
62  
63  
64  
65

1 shadows) homogeneously distributed throughout the coating layer, as confirmed by  
2  
3 EDX (Table 7). Although SiO<sub>2</sub> is an inorganic component that is also present in the frit  
4  
5 composition, when it is added to the ceramic formulation, it does not completely  
6  
7 integrate in the vitreous network, which is why a part of SiO<sub>2</sub> remains in an aggregated  
8  
9 form.

10  
11  
12 On the other hand, a new addition uniformly distributed in the ceramic formulation  
13  
14 originates a noticeable decrease in the number of bubbles, specially of small size; and  
15  
16 generates small dye aggregates (small white areas) homogeneously distributed along the  
17  
18 coating layer, as confirmed by EDX (O, Cr, Fe and Cu in more quantity). In this case  
19  
20  
21 too, the Black dye has not fully integrated in the vitreous network.  
22  
23

24  
25 These conclusions are valid for states both before and after the thermal stability test  
26  
27 (TT).  
28

29  
30 The SEM-EDX analyses obtained before and after the thermal stability test show  
31  
32 similar values in thickness as well as macroscopic and microscopic analysis, this leads  
33  
34 to a conclusion that these samples have good heat stability at thermal cycles of 550 °C  
35  
36 as expected, taking into account that thermal stability tests were performed at a  
37  
38 temperature lower than sintering temperatures, which were 780, 827 and 914 °C.  
39  
40

41  
42 The SiO<sub>2</sub> content on the coating surface was also analysed by SEM-EDX in a semi-  
43  
44 quantitative way. The results are summarised in Table 8. Sample B shows a slight  
45  
46 growth in SiO<sub>2</sub> content compared to Sample A (lower than expected in a semi-  
47  
48 quantitative assessment) as a consequence of the quartz addition in the ceramic  
49  
50 formulation. Therefore, Sample C shows lower SiO<sub>2</sub> content than Samples A and B  
51  
52 because Black dye addition decreases the overall proportionality.  
53  
54  
55  
56  
57  
58  
59  
60  
61  
62  
63  
64  
65

### 3.2.3. Influence of coating additions on optical properties

In order to determine the optical properties of the ceramic coatings, absorbance and emissivity were measured. Absorbance was analysed in the wavelength range between 780 and 2500 nm (NIR label) and emissivity in the spectral range from 2 to 20  $\mu\text{m}$  (MIR label), both at room temperature (Figure 3).

In nearly all NIR spectral range the three samples have absorbance percentages higher than 85 %. Emissivity values are around 0.9 in the MIR spectral range. These absorbance and emissivity data are comparable to other absorbers, such as a silicone-based high-temperature commercial paint (Pyromark 2500) [48].

In general, the comparison between the three ceramic coatings shows a higher absorbance percentage for Sample C at wavelengths up to 1750 nm. Above this threshold, the absorbance and emissivity of Sample C are lower than for other coatings, with the exception of a narrow wavelength band of about 9  $\mu\text{m}$ . Thus, the coating having Black dye in its composition shows spectral waveform that is different from the other coatings in the NIR region. Furthermore, Samples A and B without the Black dye component are characterised by the similar spectral curves of absorbance. The absorbance of coating with the  $\text{SiO}_2$  additive is higher than for the base formulation. In the MIR region, the emissivity curves of all samples are similar.

The differences in absolute values of absorbance for Samples A and B are caused by the different roughness levels in both samples [49] rather than by the addition of  $\text{SiO}_2$  component to the base formulation of coating. As known, a greater roughness results in a larger surface where absorption can occur. The spectral waveform in which Sample C differs from the other coatings in the spectral region up to 3  $\mu\text{m}$  is probably caused by the addition of the Black dye component. The differences are too wide and could be

1 attributed to the effect of coating roughness. The effect of the coating composition  
2  
3 rather than the roughness level is also reflected at a wavelength of about 9  $\mu\text{m}$ . The  
4  
5 difference in roughness levels of the individual samples is too low to have any effect on  
6  
7 the emissivity values [49,50].  
8  
9

10 In Figure 4, emissivity results are shown in the wavelength range from 2 to 26  $\mu\text{m}$  at a  
11  
12 temperature of 550  $^{\circ}\text{C}$ . The emissivity spectra of all coatings are similar to the  
13  
14 emissivity curves measured at room temperature. There is a slight difference in  
15  
16 emissivity Sample C at wavelengths up to 3  $\mu\text{m}$ , the emissivity is higher and the shape  
17  
18 of the spectral curve of this coating is therefore identical to the other coatings. At room  
19  
20 temperature, the differences in emissivity values of individual coatings are caused by  
21  
22 the individual composition of the coatings rather than their roughness. All spectra are  
23  
24 influenced by atmospheric absorption in the bands of 2.5 to 2.95  $\mu\text{m}$ , 4.17 to 4.5  $\mu\text{m}$ ,  
25  
26 4.8 to 7.9  $\mu\text{m}$  and from 13.2 to 17.2  $\mu\text{m}$ .  
27  
28  
29  
30  
31  
32

33 The absolute emissivity values are lower than at room temperature. The reason could  
34  
35 potentially lie in the use of different measurement methods. Therefore, it can be said  
36  
37 that the coatings do not exhibit temperature dependence and that they are temperature  
38  
39 stable. This is also supported by the results of thermal stability tests.  
40  
41  
42

43 As mentioned above, the many factors that affect heat transfer in power units include  
44  
45 the emissivity values of the device walls at its operating temperatures, wherein the  
46  
47 thermal process is supported in particular by high emissivity values of the walls.  
48  
49

50 Emissivity for room temperatures plays an important role in the initial stages of furnace  
51  
52 heating. Emissivity at high temperatures consequently contributes to the long-term  
53  
54 thermal process at the operating temperature of furnace. The band emissivity related to  
55  
56 the maximum radiated energy at the actual furnace temperature is a variable that fits the  
57  
58  
59  
60  
61  
62  
63  
64  
65

1 purpose of characterising this issue. Therefore, band normal emissivity of the coatings  
2  
3 analysed for high temperature furnace applications was calculated from spectral  
4  
5 quantities (Table 9) in the spectral band from 5  $\mu\text{m}$  to 20  $\mu\text{m}$  for room temperature and  
6  
7 in the band from 2  $\mu\text{m}$  to 9  $\mu\text{m}$  for 550  $^{\circ}\text{C}$ .  
8  
9

10 The results shown in Table 9 indicate band emissivity of all samples to be high, above  
11  
12 the value of 0.82. For room temperature, the emissivity values oscillate around 0.89.  
13  
14

15 The differences in emissivity between samples fall within the measurement uncertainty.  
16  
17

18 The results of spectral and band emissivity clearly indicate that the coatings deposited  
19  
20 by the electrophoretic deposition technique are suitable for high temperature furnace  
21  
22 applications in terms of emissivity.  
23  
24

#### 25 26 27 *3.2.4. Thermal stability of optical properties* 28

29 Absorbance was analysed in the NIR region at 1486 nm with the time after the thermal  
30  
31 stability cycles. The selected wavelength corresponds to the maximum absorbance  
32  
33 values in the NIR spectral range for all coatings. This depicts high absorbance values,  
34  
35 higher than 85 % for the three ceramic coatings (Figure 5).  
36  
37

38 The addition of  $\text{SiO}_2$  to the ceramic formulation improves the absorbance level; this  
39  
40 behaviour is even more prominent with the addition of Black dye. The explanation of  
41  
42 this behaviour resides, on the one hand, in the roughness of the samples, as it was  
43  
44 mentioned above and, on the other, in the presence of the Black dye as it absorbs more  
45  
46 due to its black nature.  
47  
48

49 The cycled tests for thermal stability reduce the long-term absorbance level of the  
50  
51 ceramic coating, especially after more than 120 hours of testing (Sample A). However,  
52  
53 the additions provide a protective effect in thermal stability (Samples B and C), which  
54  
55  
56  
57  
58  
59  
60  
61  
62  
63  
64  
65

1 aids in keeping the long-term absorbance level more stable for the studied range of  
2  
3  
4 wavelengths.  
5  
6

#### 7 **4. Conclusions**

8  
9

10 High emissivity ceramic coatings obtained by EPD were designed to use in the inner  
11 walls or superheaters and metallic structures of furnaces with the aim of considerably  
12 improving heat transfer, to deliver important energy savings, and to maximise the  
13 efficiency of such equipment. . The characterisation tests performed have provided the  
14 conclusions below:  
15  
16  
17  
18  
19  
20  
21

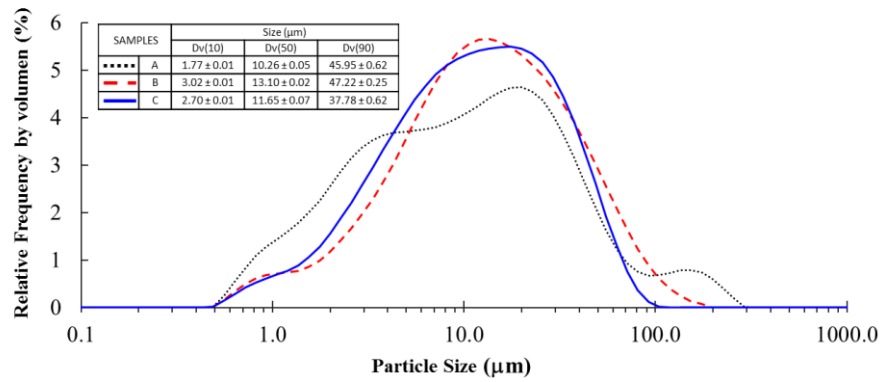
- 22 1. The ceramic formulations have a suitable and homogeneous particle size  
23 distribution to be applied by EPD technique.  
24  
25
- 26 2. The SiO<sub>2</sub> addition moves the characteristic temperatures to upper ranges (by  
27 more than 40 °C) as SiO<sub>2</sub> is a component that remains stable at high  
28 temperatures. The Black dye, which is based on metallic oxides with high  
29 melting points (Fe, Cr and Cu), allows to increase the characteristic temperatures  
30 by more than 130 °C as a consequence of the excellent chemical stability of such  
31 metallic oxides.  
32  
33
- 34 3. No significant changes can be detected with the SiO<sub>2</sub> and Black dye addition in  
35 terms of adherence due to the good quality of chemical bonding established in  
36 the steel-ceramic coating interface.  
37  
38
- 39 4. Thermal stability test indicates more surfaces with a higher roughness for all  
40 cases. The additions, SiO<sub>2</sub> and Black dye, provide a greater protective effect due  
41 to their refractory nature and their not being embedded in the vitreous net, which  
42 contributes to increasing the surface roughness.  
43  
44  
45  
46  
47  
48  
49  
50  
51  
52  
53  
54  
55  
56  
57  
58  
59  
60  
61  
62  
63  
64  
65



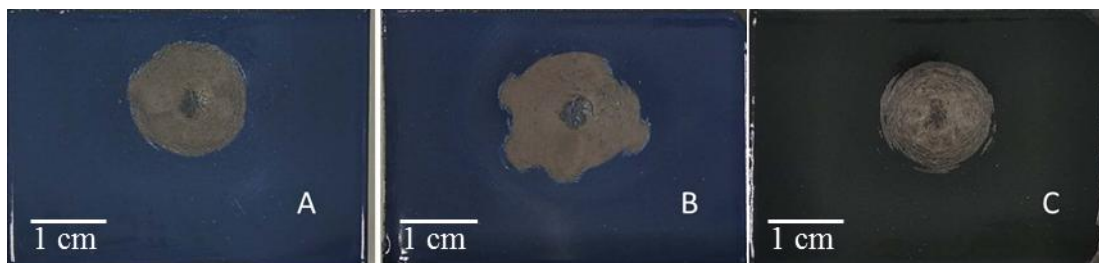
- 1 5. Coating thickness is not affected by the thermal stability test and the bubble  
2 structure remains confined in the coating thickness showing slight differences  
3  
4 between the three samples. The addition of SiO<sub>2</sub> reduces the number of bubbles  
5  
6 and generates SiO<sub>2</sub> aggregates homogeneously distributed throughout the  
7  
8 coating layer. An additional introduction of Black dye considerably decreases  
9  
10 the number of small bubbles and generates small dye aggregates which are  
11  
12 homogeneously distributed as well.  
13  
14  
15  
16  
17
- 18 6. In nearly all NIR spectral ranges, the three samples show absorbance  
19  
20 percentages higher than 85 %. The addition of SiO<sub>2</sub> improves the absorbance  
21  
22 level due to increased roughness; the effect becomes more pronounced with the  
23  
24 addition of Black dye owing to its black nature. Besides, the additions provide a  
25  
26 protective effect in the thermal stability of the coatings while maintaining the  
27  
28 absorbance level more stable in the long term.  
29  
30  
31
- 32 7. In the MIR spectral range, emissivity values oscillate around 0.89 at room  
33  
34 temperature; the slight differences between the three samples derive from the  
35  
36 coating composition rather than the roughness level. There is a slight reduction  
37  
38 of emissivity result at 550 °C, around 0.82 for all coatings.  
39  
40  
41  
42

43 The vitreous ceramic coatings obtained by the electrophoretic deposition technique meet  
44 the requirements of high thermal stability and high emissivity. Therefore, the EPD  
45  
46 technique is suitable for preparing coatings intended for metallic components placed  
47  
48 inside furnaces.  
49  
50  
51  
52  
53  
54  
55  
56  
57  
58  
59  
60  
61  
62  
63  
64  
65

1 Figure 1. Particle size of ceramic formulations: A (Blank), B (Blank + SiO<sub>2</sub>), C (Blank  
 2  
 3 + SiO<sub>2</sub> + Black dye).  
 4  
 5  
 6  
 7  
 8  
 9



1 Figure 2. Adherence test results of the coatings: A) Blank; B) Blank + SiO<sub>2</sub>; and C)  
2  
3 Blank + SiO<sub>2</sub> + Black dye.  
4  
5



1 Figure 3. (a) Absorption spectra of the coatings. (b) Spectral emissivity of the coatings  
2  
3  
4 at room temperature.  
5  
6

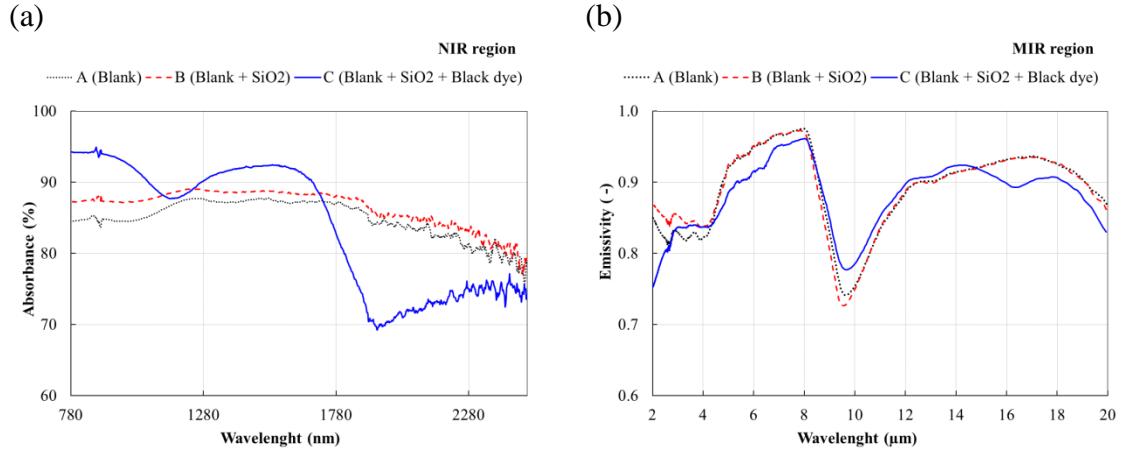
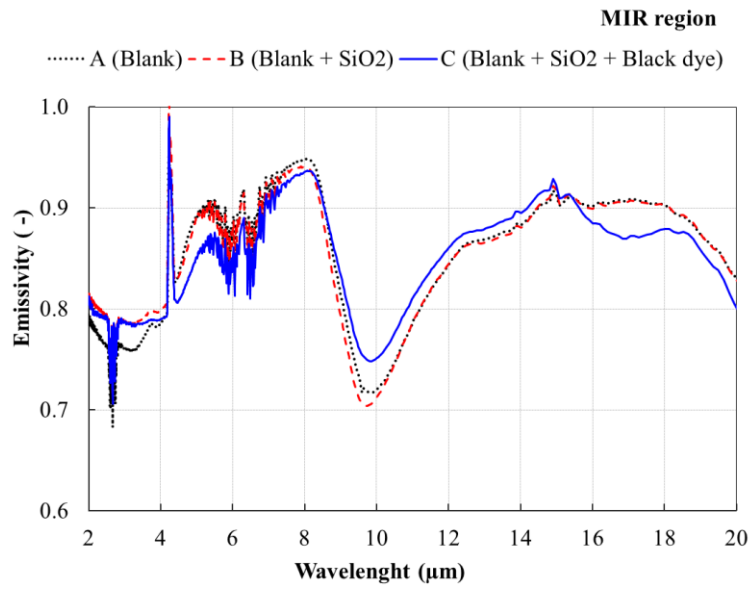


Figure 4. Spectral emissivity of the coatings at temperature of 550 °C.



1 Figure 5. Absorbance vs. thermal cycles' time at 1486 nm (NIR) wavelength of the  
2  
3 coatings.  
4  
5

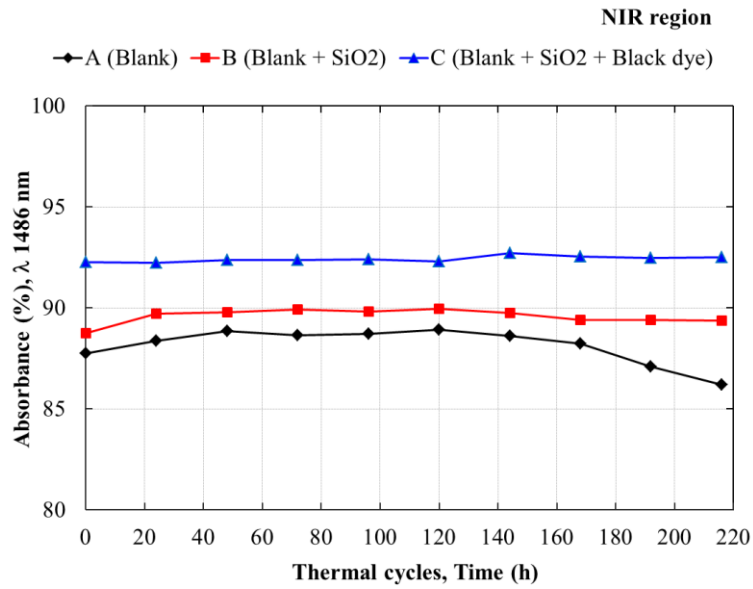


Table 1. Heating microscope characterisation of formulations.






Sample	Sintering 	Softening 	Sphere 	Half Sphere 	Melting Point 
<b>A</b> <b>Blank</b>	590 °C	668 °C	712 °C	753 °C	780 °C
<b>B</b> <b>Blank + SiO<sub>2</sub></b>	589 °C	658 °C	770 °C	797 °C	827 °C
<b>C</b> <b>Blank + SiO<sub>2</sub> + Black dye</b>	595 °C	704 °C	823 °C	864 °C	914 °C

Table 2. Reactions during firing of first layer of ceramic coatings on steel [44].

STEEL	CERAMIC COATING
Oxidation $\text{Fe} \rightarrow \text{Fe}^{2+}/\text{Fe}^{3+}$	Degassing of biscuit $\text{H}_2\text{O}\uparrow$
Degassing / decomposition of oil residues, $\text{H}_2$ , $\text{CO}$ , $\text{CO}_2$	Decomposition of mill additions
Wetting by vitreous ceramic coating favoured by Fe, Co, Cu	“Melting” of vitreous ceramic coating – depending on glass structure
Formation of Fe-oxidation	Diffusion of alkali ions, $\text{F}^-$ , $\text{Co}^{2+}$ and $\text{Fe}^{2+}$
Changes of metallurgical structure (grains, phases)	Saturation of $\text{FeO}$ / $\text{Fe}_3\text{O}_4$ at the ceramic coating steel interface, $\text{O}_2$ -penetration
Formation of $\text{Fe}_x\text{Co}_y$ dendrites (anchor points between ceramic coating and substrate)	



Table 3. Coatings surface after thermal stability tests, macroscopic (36 mm x 50 mm x 1 mm) and microscopic analysis (16.3 x magnification).




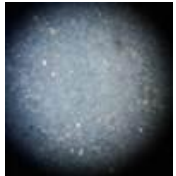














	<b>A Blank</b>		<b>B Blank +SiO<sub>2</sub></b>		<b>C Blank + SiO<sub>2</sub> + Black dye</b>	
<b>Time</b>	Macroscopic level	Microscopic level	Macroscopic level	Microscopic level	Macroscopic level	Microscopic level
<b>0h</b>						
<b>120h</b>						
<b>216h</b>						

Table 4. 3D surface roughness morphology of the coatings.

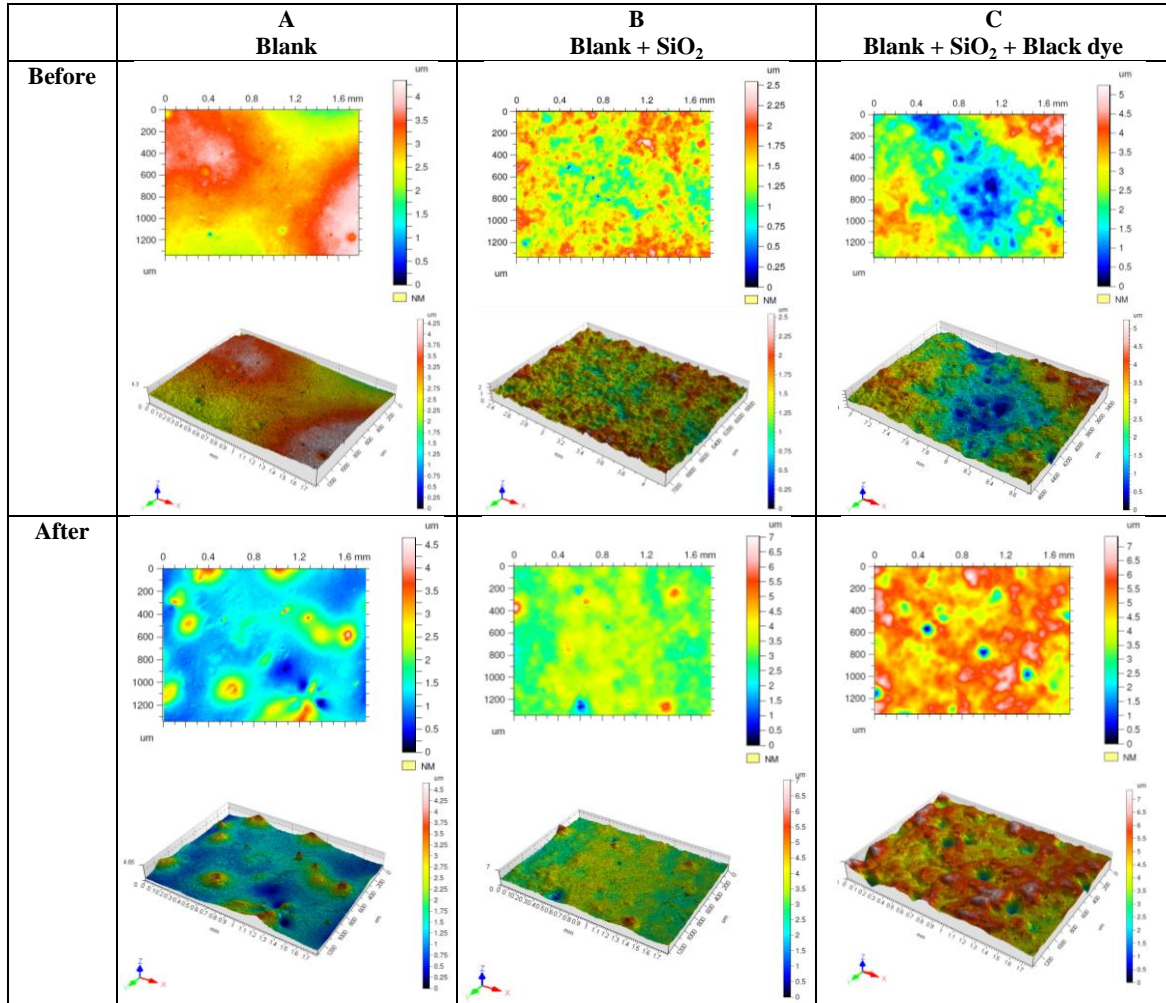


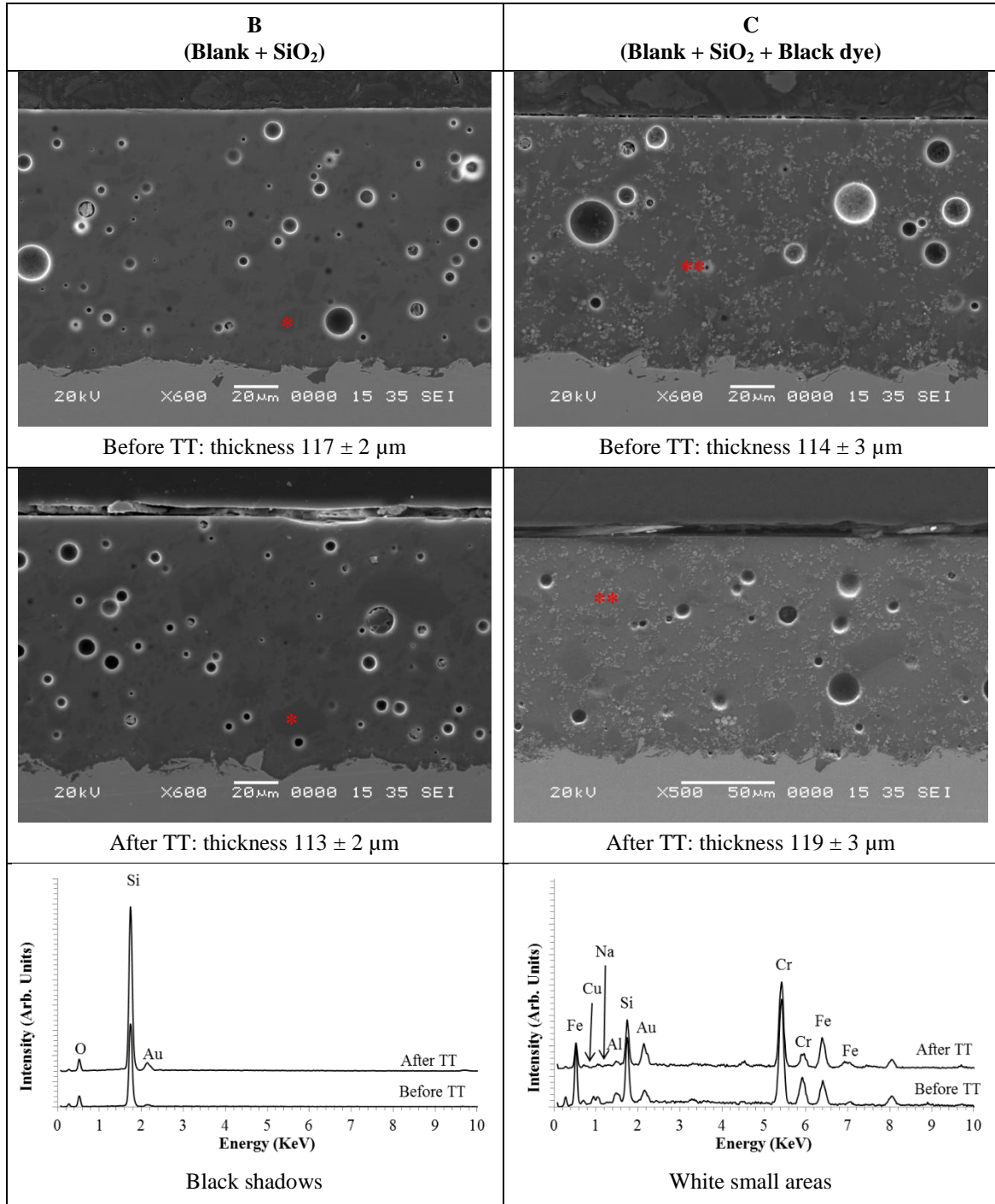
Table 5. Surface roughness, Ra ( $\mu\text{m}$ ) of the coatings.

<b>A Blank</b>		<b>B Blank + SiO<sub>2</sub></b>		<b>C Blank + SiO<sub>2</sub> + Black dye</b>	
<b>Before</b>	<b>After</b>	<b>Before</b>	<b>After</b>	<b>Before</b>	<b>After</b>
0.021 $\pm$ 0.003	0.168 $\pm$ 0.086	0.141 $\pm$ 0.027	0.207 $\pm$ 0.079	0.214 $\pm$ 0.042	0.355 $\pm$ 0.125

Table 6. SEM/EDX mapping analysis and semi-quantitative determination of silicon (Si), iron (Fe), chromium (Cr) and copper (Cu) of the coatings.

		SEM	Si	Fe	Cr	Cu
Before	A					
	B					
	C					
After	A					
	B					
	C					

Table 7. Cross-sectional SEM micrographs of B and C coatings and EDX of shadows:  
 black for Sample B and white for Sample C.



1 Table 8. Semi-quantitative assessment of SiO<sub>2</sub> content on surface by EDX  
 2  
 3

4 microanalysis technique before and after thermal stability tests of the coatings.  
 5  
 6

Nominal SiO <sub>2</sub> (wt%)	A Blank		B Blank + SiO <sub>2</sub>		C Blank + SiO <sub>2</sub> + Black dye	
	Before	After	Before	After	Before	After
SiO <sub>2</sub> on surface	72.41 ± 1.75	73.20 ± 1.75	75.40 ± 1.08	76.99 ± 1.49	62.78 ± 1.00	62.16 ± 1.42

Table 9. Band normal emissivity at room temperature in spectral band from 5  $\mu\text{m}$  to 20  $\mu\text{m}$  and at temperature of 550  $^{\circ}\text{C}$  in spectral band from 2  $\mu\text{m}$  to 9  $\mu\text{m}$ .

<b>T (<math>^{\circ}\text{C}</math>)</b>	<b>A Blank</b>	<b>B Blank + SiO<sub>2</sub></b>	<b>C Blank + SiO<sub>2</sub> + Black dye</b>
<b>Troom</b> $\lambda$ 5 – 20 $\mu\text{m}$	<b><i>0.892</i> <math>\pm</math> 0.027</b>	<b><i>0.889</i> <math>\pm</math> 0.027</b>	<b><i>0.890</i> <math>\pm</math> 0.027</b>
<b>550 <math>^{\circ}\text{C}</math></b> $\lambda$ 2 – 9 $\mu\text{m}$	<b><i>0.835</i> <math>\pm</math> 0.029</b>	<b><i>0.838</i> <math>\pm</math> 0.029</b>	<b><i>0.820</i> <math>\pm</math> 0.029</b>

## Acknowledgements

The authors thank both the Economic development and Competitiveness Department of the Basque Government (ELKARTEK BEROA-GO 2.0 0 project reg. no. KK-2017/00060 and ELKARTEK FRONTIERS IV project reg. no. KK-2018/00108) and the Ministry of Education, Youth and Sport of the Czech Republic (LabIR-PAV project reg. no. CZ.02.1.01/0.0/0.0/18\_069/0010018) for partially supporting this research.



## References

- [1] Energy Efficiency, European Commission topics, <https://ec.europa.eu/energy/en/topics/energy-efficiency>, 2019.
- [2] G.J. Heynderickx, M. Nozawa, High-emissivity coatings on reactor tubes and furnace walls in steam cracking furnaces, *Chem. Eng. Sci.* 59 (2004) 5657-5662, <https://doi.org/10.1016/j.ces.2004.07.075>.
- [3] A. Martenson, Energy efficiency improvement by and control: A case study of reheating furnaces in the steel industry, Proceedings from the 14th National Industrial Energy Technology Conference, Houston, Texas, USA, April 22-23, 1992, <http://hdl.handle.net/1969.1/92210>.
- [4] J.C. Hellander, Throughput enhancement and tube temperature stabilization, *Hydrocarbon Processing*, November 1997.
- [5] J.D. Jackson, Y. Chien-Cheng, Measurements of total and spectral emissivities of some ceramic fiber insulation materials, *Ceram. Energy Appl., Proc. Inst. Energy's Int. Conf., 2<sup>nd</sup>*, Pergamon Press, London, 1994, pp. 159–174, <https://doi.org/10.1016/B978-0-08-042133-9.50016-2>.
- [6] J.D. Jackson, P. An, I. Pena-Marco, 1995. Measurement of the total and spectral emittance of permeable ceramic materials, *Proc. 4th UK National Heat Transfer Conference, C510/132/95, IMechE (1995)* 561-565.
- [7] X. He, Y. Li, L. Wang, Y. Sun, S. Zhang, High emissivity coatings for high temperature application: Progress and prospect, *Thin Solid Films* 517 (2009) 5120-5129, <https://doi.org/10.1016/j.tsf.2009.03.175>.

- 1 [8] M. Mauer, P. Kalenda, M. Honner, P. Vacikova, Composite fillers and their  
2 influence on emissivity, *J. Phys. Chem. Solids* 73 (2012) 1550-1555,  
3  
4  
5  
6 <https://doi.org/10.1016/j.jpcs.2011.11.015>.  
7
- 8 [9] Institute of Energy, London, *Ceramics in energy applications*, Adam Hilger, Bristol  
9 and New York, 1990.
- 10  
11  
12  
13 [10] B.V. Cockeram, D.P. Measures, A.J. Mueller, The development and testing of  
14 emissivity enhancement coatings for thermophotovoltaic TPV radiator applications,  
15  
16  
17  
18 *Thin Solid Films*, 355–356 (1999) 17-25, [https://doi.org/10.1016/S0040-](https://doi.org/10.1016/S0040-6090(99)00438-1)  
19  
20  
21  
22 [6090\(99\)00438-1](https://doi.org/10.1016/S0040-6090(99)00438-1).
- 23 [11] Z. Dan, D. Cang, H. Zhou, H. Bai, Y. Zong, Microstructure and properties of high  
24 emissivity coatings, *J. Univ. Sci. Technol. Beijing* 15 (2008) 627-632,  
25  
26  
27  
28 [https://doi.org/10.1016/S1005-8850\(08\)60117-6](https://doi.org/10.1016/S1005-8850(08)60117-6).  
29
- 30 [12] M.G. Hocking, V. Vasantasree, P.S. Sidky, *Metallic and ceramic coatings:*  
31  
32  
33  
34  
35  
36  
37  
38  
39  
40  
41  
42  
43  
44  
45  
46  
47  
48  
49  
50  
51  
52  
53  
54  
55  
56  
57  
58  
59  
60  
61  
62  
63  
64  
65
- [13] M. Falz, G. Leonhardt, PVD coatings with high IR emissivity for high temperature applications of Co-based alloys, *Surf. Coat. Technol.* 61 (1993) 97-100,  
[https://doi.org/10.1016/0257-8972\(93\)90209-7](https://doi.org/10.1016/0257-8972(93)90209-7).
- [14] C. Bartuli, T. Valente, M. Tului, Plasma spray deposition and high temperature characterization of ZrB<sub>2</sub>–SiC protective coatings, *Surf. Coat. Technol.* 155 (2002) 260-273, [https://doi.org/10.1016/S0257-8972\(02\)00058-0](https://doi.org/10.1016/S0257-8972(02)00058-0).
- [15] J. Yi, X.D. He, Y. Sun, Y. Li, Electron beam-physical vapor deposition of SiC/SiO<sub>2</sub> high emissivity thin film, *Appl. Surf. Sci.* 253 (2007) 4361-4366,  
<https://doi.org/10.1016/j.apsusc.2006.09.063>.

- 1 [16] T. Kralik, D. Katsir, Black surfaces for infrared, aerospace and cryogenic  
2 applications, Proc. SPIE 7298, Infrared Technology and Applications XXXV, 729813  
3  
4 (2009), <https://doi.org/10.1117/12.819277>.  
5  
6  
7  
8 [17] D. Cárdenas-García, Emissivity measurement of high-emissivity black paint at  
9 CENAM, Rev. Mex. Fis. 60 (2014) 305-308,  
10  
11 <http://www.scielo.org.mx/pdf/rmf/v60n4/v60n4a10.pdf>.  
12  
13  
14 [18] M. Švantner, P. Honnerová, Z. Veselý, The influence of furnace wall emissivity on  
15 steel charge heating, Infrared Phys. Technol. 74 (2016) 63-71,  
16  
17 <https://doi.org/10.1016/j.infrared.2015.12.001>.  
18  
19  
20 [19] G.D. Stefanidis, K.M. Van Gee, G.J. Heynderickx, G.B. Marin, Evaluation of high-  
21 emissivity coatings in steam cracking furnaces using a non-grey gas radiation model,  
22 Chem. Eng. J. 137 (2008) 411-421, <https://doi.org/10.1016/j.cej.2007.04.04>.  
23  
24  
25 [20] J.C. Hellander, Ceramic coat furnace tubes for improved operations, Hydrocarbon  
26 Process., Int. Ed. 76 (1997) 91-96.  
27  
28 [21] P.M. Martin, Handbook of deposition technologies for films and coatings: science,  
29 applications and technology, 3<sup>rd</sup> Ed. 2010.  
30  
31 [22] L. Besra, M. Liu, A review on fundamentals and applications of electrophoretic  
32 deposition (EPD), Prog. Mater. Sci. 52 (2007) 1–61,  
33  
34 <https://doi.org/10.1016/j.pmatsci.2006.07.001>.  
35  
36 [23] S. Morelli, R. Pérez, A. Querejeta, J. Muñoz, L. Lusvarghi, M.L. Gualteri, G.  
37 Bolelli, H.J. Grande, Photocatalytic enamel/TiO<sub>2</sub> coatings developed by electrophoretic  
38 deposition for methyl orange decomposition, Ceram. Int. 44 (2018) 16199-16208,  
39  
40  
41  
42  
43  
44  
45 <https://doi.org/10.1016/j.ceramint.2018.05.245>.  
46  
47  
48  
49  
50  
51  
52  
53  
54  
55  
56  
57  
58  
59  
60  
61  
62  
63  
64  
65

- 1 [24] C. L. Sparreo, R. Vanderberg, Application of porcelain enamel by the  
2  
3 electrophoretic enamelling process, *Ceram. Eng. Sci. Proc.* 19 (1998) 151-157,  
4  
5 <https://doi.org/10.1002/9780470294512.ch27>.  
6  
7
- 8 [25] D. Vélez, J. Muñoz, J.A. Díez, Influence of application technology in the structural  
9  
10 characteristics of ceramic coating with advanced anticorrosive and tribological  
11  
12 properties, *Adv. Sci. Tech.* 91 (2014) 108-116,  
13  
14 <https://doi.org/10.4028/www.scientific.net/AST.91.108>  
15  
16
- 17 [26] B. Micó-Vicent, M. López-Herraiz, A. Bello, N. Martínez, F.M. Martínez-Verdú,  
18  
19 Synthesis of pillared clays from metallic salts as pigments for thermosolar absorptive  
20  
21 coatings, *Sol. Energy* 155 (2017) 314-322,  
22  
23 <https://doi.org/10.1016/j.solener.2017.06.034>.  
24  
25
- 26 [27] M. Massoud, *Engineering Thermofluids: Thermodynamics, Fluid Mechanics, and*  
27  
28 *Heat Transfer*, 2005.  
29  
30
- 31 [28] S. Rossi, M. Calovi, D. Vélez, J. Muñoz, Influence of addition of hard particles on  
32  
33 the mechanical and chemical behavior of vitreous enamel, *Surf. Coat. Tech.* 357 (2019)  
34  
35 69-77, <https://doi.org/10.1016/j.surfcoat.2018.09.062>.  
36  
37
- 38 [29] ISO 3310-1 Test sieves -- Technical requirements and testing -- Part 1: Test sieves  
39  
40 of metal wire cloth, <https://www.iso.org/standard/62410.html>, 2016.  
41  
42
- 43 [30] M.R. Pérez García, J. Muñoz, J.A. Díez, Taguchi experimental design method for  
44  
45 electrophoretic porcelain enamel (EPE), *ECerS 2015 14th International Conference –*  
46  
47 *European Ceramic Society*  
48  
49
- 50 [31] DIN 51730 Testing of solid fuels; determination of fusibility of fuel ash,  
51  
52 [https://global.ihs.com/doc\\_detail.cfm?document\\_name=DIN%2051730&items\\_key=0](https://global.ihs.com/doc_detail.cfm?document_name=DIN%2051730&items_key=0124624)  
53  
54 [0124624](https://global.ihs.com/doc_detail.cfm?document_name=DIN%2051730&items_key=0124624), 1998.  
55  
56  
57  
58  
59  
60  
61  
62  
63  
64  
65

- 1 [32] UNE-EN 10209 Cold rolled low carbon steel flat products for vitreous enamelling -  
2  
3 Technical delivery conditions, [https://www.une.org/encuentra-tu-norma/busca-tu-](https://www.une.org/encuentra-tu-norma/busca-tu-norma/norma?c=N0052188)  
4  
5 [norma/norma?c=N0052188](https://www.une.org/encuentra-tu-norma/busca-tu-norma/norma?c=N0052188), 2013.  
6  
7  
8 [33] P. Honnerová, J. Martan, Z. Veselý, M. Honner, Method for emissivity  
9  
10 measurement of semitransparent coatings at ambient temperature, Sci. Rep. 7 (2017)  
11  
12 1386 (14pp), <https://doi.org/10.1038/s41598-017-01574-x>.  
13  
14  
15 [34] M.J. Riedl, Optical design fundamentals for infrared systems, 2<sup>nd</sup> Ed. 2001,  
16  
17 <https://doi.org/10.1117/3.412729>.  
18  
19  
20 [35] P. Honnerová, J. Martan, M. Kučera, M. Honner, J. Hameury, New experimental  
21  
22 device for high-temperature normal spectral emissivity measurements of coatings,  
23  
24 Meas. Sci. Technol. 25 (2014) 095501 (9pp), [http://dx.doi.org/10.1088/0957-](http://dx.doi.org/10.1088/0957-0233/25/9/095501)  
25  
26 [0233/25/9/095501](http://dx.doi.org/10.1088/0957-0233/25/9/095501).  
27  
28  
29 [36] J. R. Howell, M. Pinar Menguc, R. Siegel, Thermal radiation heat transfer, Taylor  
30  
31 & Francis Group 5<sup>th</sup> Ed., London, 2010, <https://doi.org/10.1201/9781439894552>.  
32  
33  
34 [37] P. Amrollahi, J. Krasinski, R.K. Vaidyanathan, L. Tayebi, D. Vashae, 7  
35  
36 Electrophoretic deposition (EPD): fundamentals and applications from nano-to micro-  
37  
38 scale structures, Handbook of Nanoelectrochemistry, (2015) 561-591,  
39  
40 [https://doi.org/10.1007/978-3-319-15266-0\\_7](https://doi.org/10.1007/978-3-319-15266-0_7).  
41  
42  
43 [38] X. Yang, A. Jha, R. Brydson, R.C. Cochrane, An analysis of the microstructure and  
44  
45 interfacial chemistry of steel-enamel interface, Thin Solid Films 443 (2003) 33-45,  
46  
47 [https://doi.org/10.1016/S0040-6090\(03\)00973-8](https://doi.org/10.1016/S0040-6090(03)00973-8).  
48  
49  
50 [39] M. Peterson, A.M. Bernardin, N. Cabral Kuhnen, H. Gracher Riella, Evaluation of  
51  
52 the steger method in the determination of ceramic-glaze joining, Mater. Sci. Eng., A  
53  
54  
55 466 (2007) 183-186, <https://doi.org/10.1016/j.msea.2007.02.046>.  
56  
57  
58  
59  
60  
61  
62  
63  
64  
65

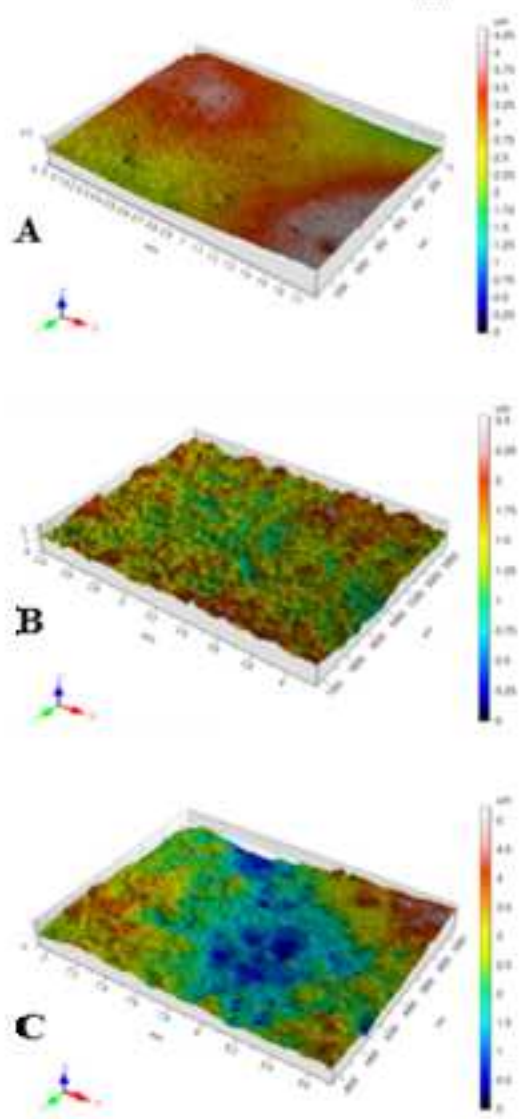
- 1 [40] A. Zucchelli, G. Minak, D. Ghelli, Low-velocity impact behavior of vitreous-  
2 enameled steel plates, Int. J. Impact Eng. 37 (2010) 673-684,  
3  
4  
5  
6 <https://doi.org/10.1016/j.ijimpeng.2009.12.003>.  
7
- 8 [41] D. Ritchie, H.A. Schaeffer, D. White, The presence of an iron oxide layer at the  
9 enamel-steel interface in one-coat porcelain enamelling, J. Mater. Sci. 18 (1983) 599-  
10  
11  
12  
13 604, <https://doi.org/10.1007/BF00560649>.  
14
- 15 [42] E. Paparazzo, G. Fierro, G.M. Ingo, S. Sturlse, Microchemistry and mechanisms of  
16 adherence in steel-enamel interface, J. Am. Ceram. Soc. 71 (1988) C494,  
17  
18  
19  
20  
21 <https://doi.org/10.1111/j.1151-2916.1988.tb05816.x>.  
22
- 23 [43] S. Rossi, M. Calovi, D. Vélez, I. Rodríguez, M. del Rincón, J.M. Muñoz, H.J.  
24 Grande, Microstructural analysis and surface modification of a vitreous enamel  
25 modified with corundum particles, Adv. Eng. Mater. (2019) 1900231  
26  
27  
28  
29  
30  
31 <https://doi.org/10.1002/adem.201900231>.  
32
- 33 [44] Pemco Enamel Manual. 2<sup>nd</sup> Ed. Pemco Brugge, Belgium 2008. ISBN 978-90-  
34  
35 9022988-1.  
36
- 37 [45] S. Pagliuca, W.D.Faust, Porcelain (vitreous) enamels and industrial enamelling  
38 processes 3<sup>rd</sup> Ed., The International Enamellers Institute, Mantova 2011.  
39
- 40 [46] W. E. Matthes, Keramische Glasuren. In: Grundlagen, Eigenschaften, Rezepte,  
41 Anwendung, 2<sup>nd</sup> Ed., Augustus-Verlag, Augsburg, 1990.  
42  
43  
44
- 45 [47] A. Petzold, H. Pöschmann, Email und emailiertechnik, 2<sup>nd</sup> Ed., Deutscher Verlag  
46 für Grundstoffindustrie, Leipzig, 1992.  
47  
48  
49  
50
- 51 [48] C. K. Ho, A. R. Mahoney, A. Ambrosini, M. Bencomo, A. Hall, T. N. Lambert,  
52  
53  
54  
55  
56  
57  
58  
59  
60  
61  
62  
63  
64  
65
- Characterization of Pyromark 2500 paint for high-temperature solar receivers, J. Sol.  
Energy Eng. 136 (2014) 014502, <https://doi.org/10.1115/1.4024031>.

- 1 [49] K. Malnieks, G. Mezinskis, I. Pavlovska, L. Bidermanis, A. Pludons, Black enamel  
2  
3 for concentrated solar-power receivers, *Ceramics International* 40 (2014) 13321-13327,  
4  
5 <https://doi.org/10.1016/j.ceramint.2014.05.046>.  
6  
7  
8 [50] E. Brodu, M. Balat-Pichelin, J.L. Sans, M.D. Freeman, J.C. Kasper, Efficiency and  
9  
10 behaviour of textured high emissivity metallic coatings at high temperature, *Mater. Des.*  
11  
12 83 (2015) 85–94, <https://doi.org/10.1016/j.matdes.2015.05.073>.  
13  
14  
15  
16  
17  
18  
19  
20  
21  
22  
23  
24  
25  
26  
27  
28  
29  
30  
31  
32  
33  
34  
35  
36  
37  
38  
39  
40  
41  
42  
43  
44  
45  
46  
47  
48  
49  
50  
51  
52  
53  
54  
55  
56  
57  
58  
59  
60  
61  
62  
63  
64  
65

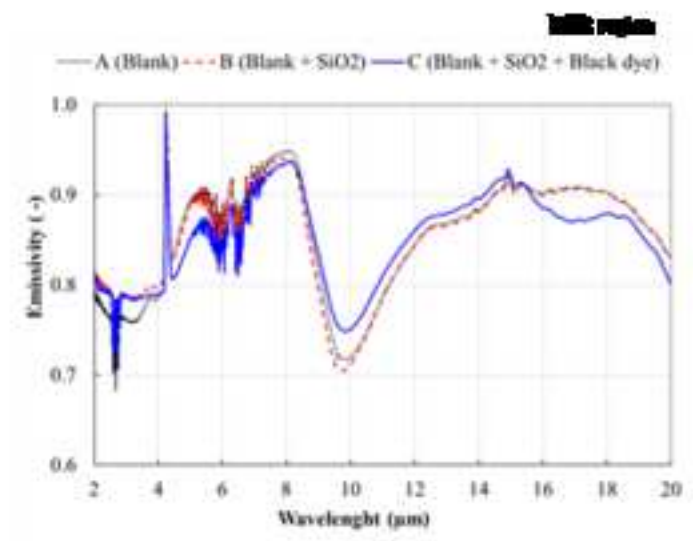
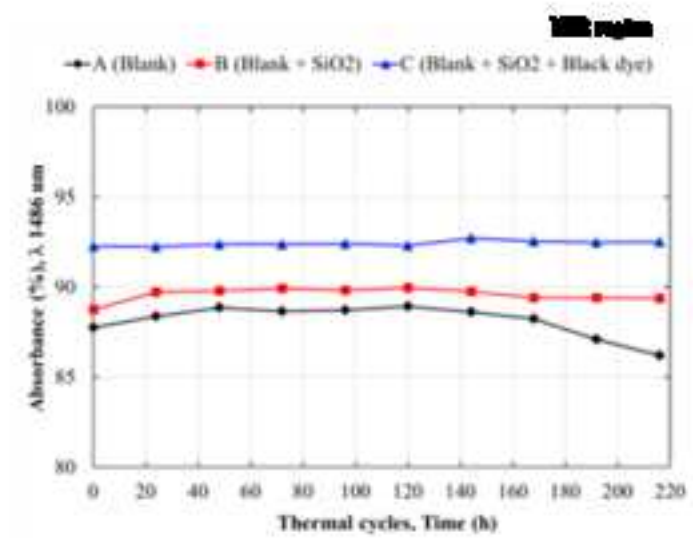
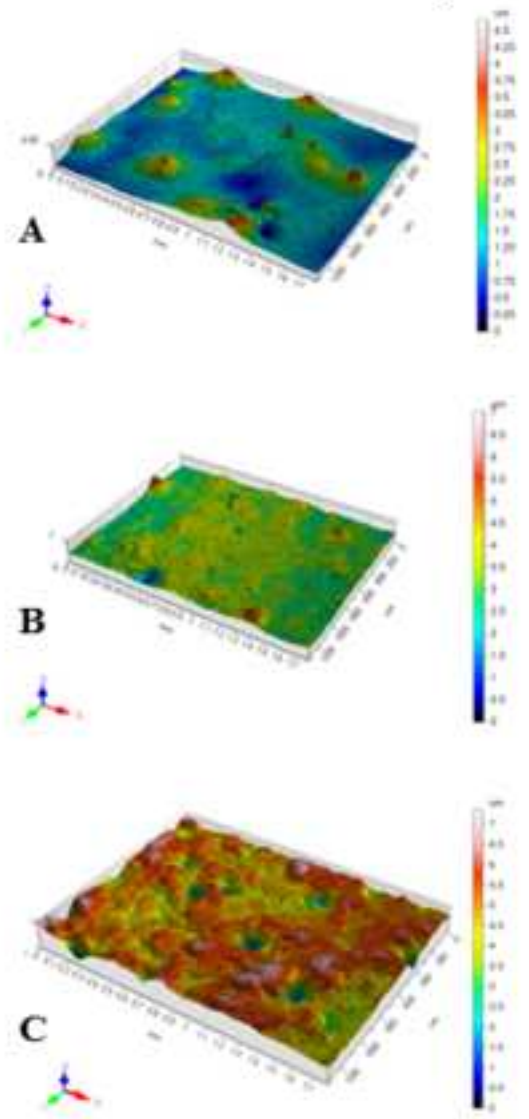
Figure

[Click here to download high resolution image](#)

### Before thermal stability



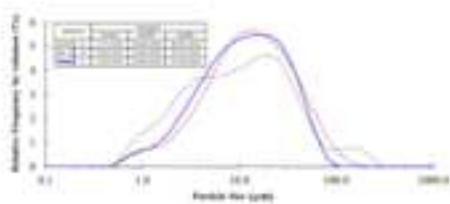
### After thermal stability





# Figure

[Click here to download high resolution image](#)



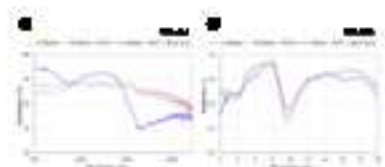
# Figure

[Click here to download high resolution image](#)



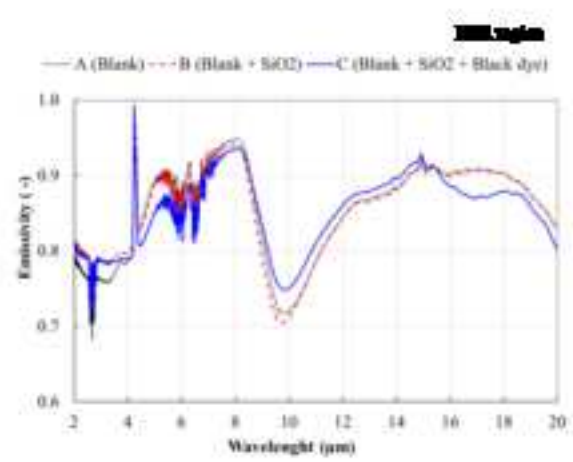
# Figure

[Click here to download high resolution image](#)



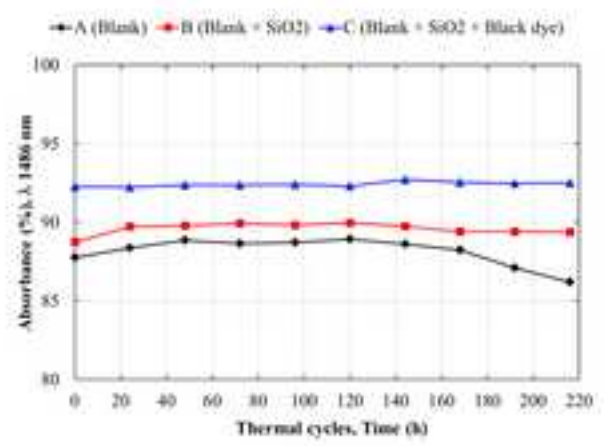
# Figure

[Click here to download high resolution image](#)








# Figure

[Click here to download high resolution image](#)



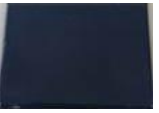






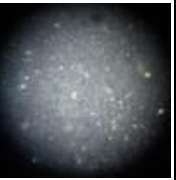

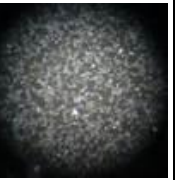

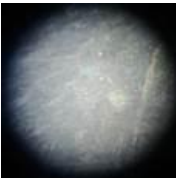

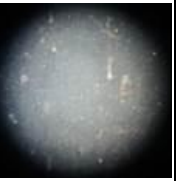

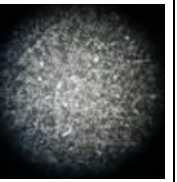


Table

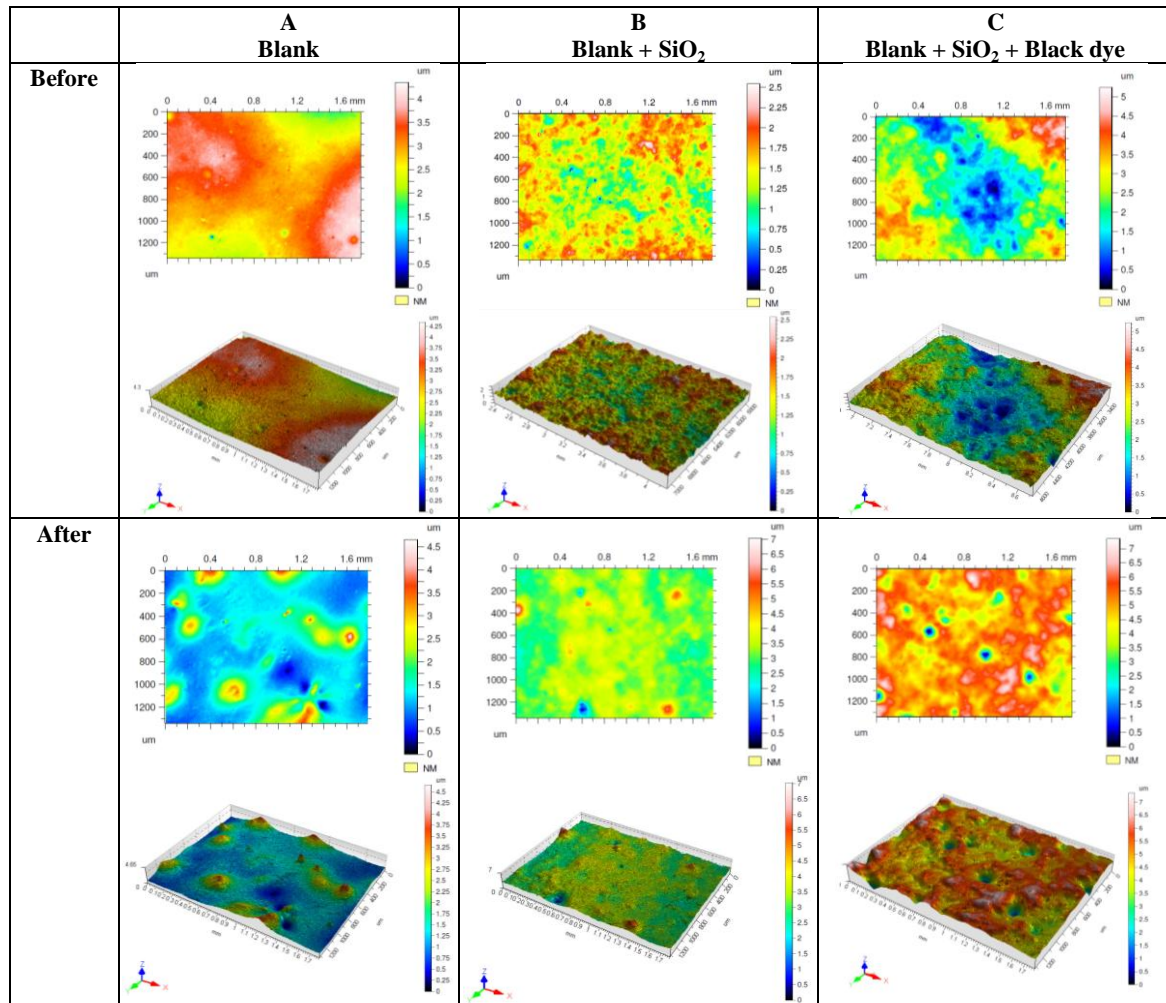
Sample	Sintering 	Softening 	Sphere 	Half Sphere 	Melting Point 
<b>A</b> Blank	590 °C	668 °C	712 °C	753 °C	780 °C
<b>B</b> Blank + SiO <sub>2</sub>	589 °C	658 °C	770 °C	797 °C	827 °C
<b>C</b> Blank + SiO <sub>2</sub> + Black dye	595 °C	704 °C	823 °C	864 °C	914 °C

STEEL	CERAMIC COATING
Oxidation $\text{Fe} \rightarrow \text{Fe}^{2+}/\text{Fe}^{3+}$	Degassing of biscuit $\text{H}_2\text{O}\uparrow$
Degassing / decomposition of oil residues, $\text{H}_2$ , $\text{CO}$ , $\text{CO}_2$	Decomposition of mill additions
Wetting by vitreous ceramic coating favoured by $\text{Fe}$ , $\text{Co}$ , $\text{Cu}$	“Melting” of vitreous ceramic coating – depending on glass structure
Formation of Fe-oxidation	Diffusion of alkali ions, $\text{F}^-$ , $\text{Co}^{2+}$ and $\text{Fe}^{2+}$
Changes of metallurgical structure (grains, phases)	Saturation of $\text{FeO}$ / $\text{Fe}_3\text{O}_4$ at the ceramic coating steel interface, $\text{O}_2$ -penetration
Formation of $\text{Fe}_x\text{Co}_y$ dendrites (anchor points between ceramic coating and substrate)	

Table

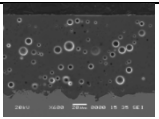
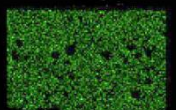
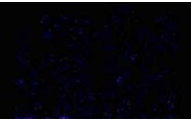

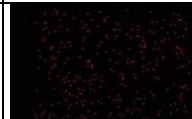
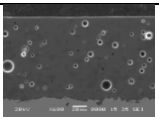
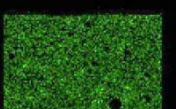



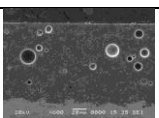
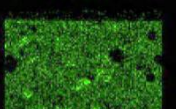



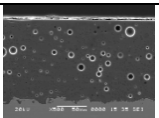
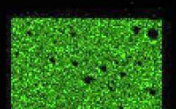
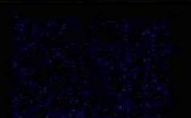
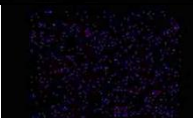

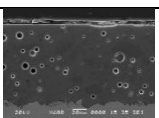
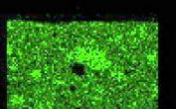

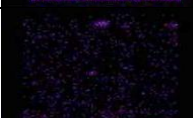

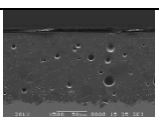
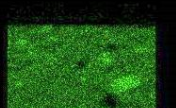



	<b>A Blank</b>		<b>B Blank +SiO<sub>2</sub></b>		<b>C Blank + SiO<sub>2</sub> + Black dye</b>	
<b>Time</b>	Macroscopic level	Microscopic level	Macroscopic level	Microscopic level	Macroscopic level	Microscopic level
<b>0h</b>						
<b>120h</b>						
<b>216h</b>						

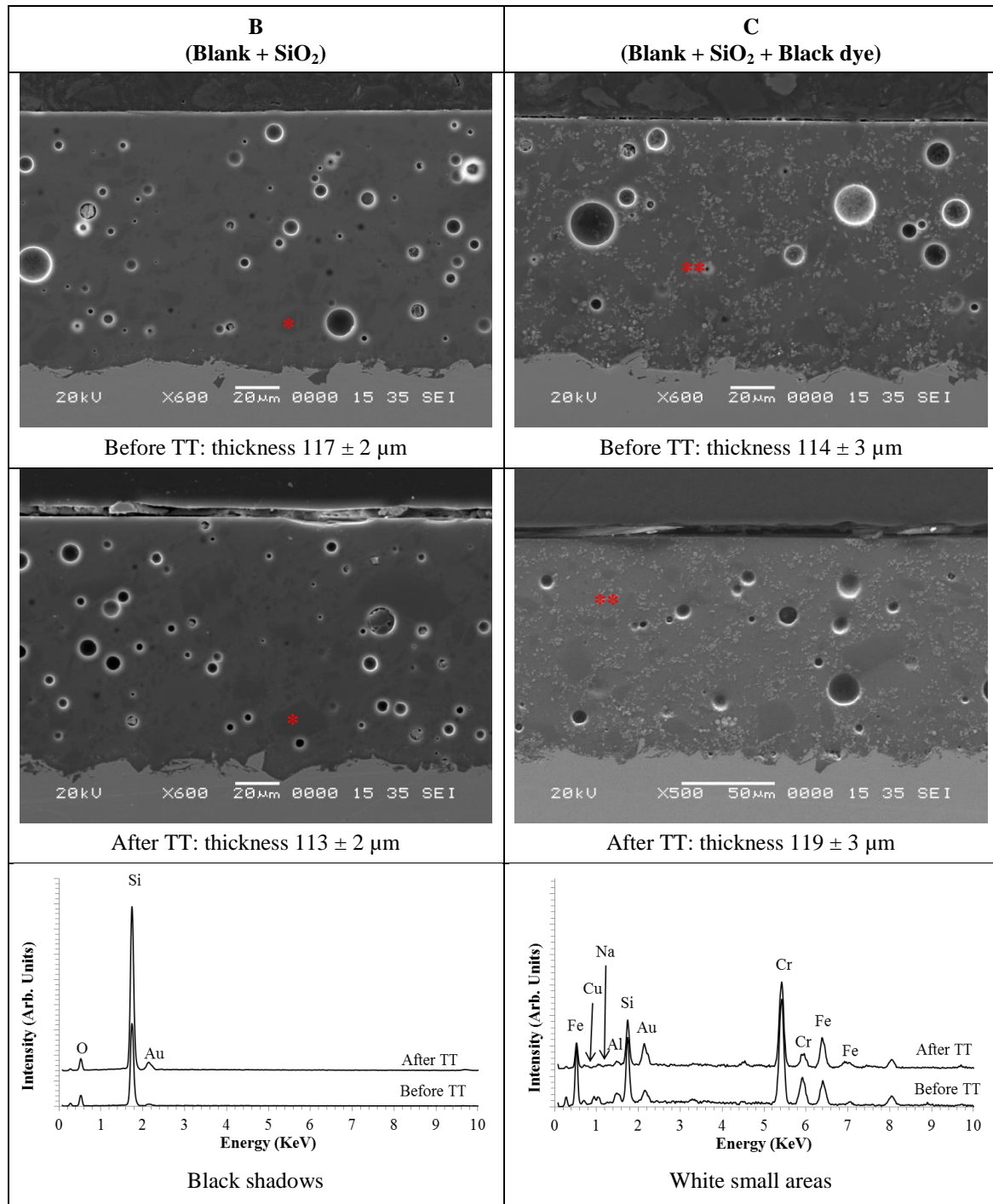




**Table**

<b>A Blank</b>		<b>B Blank + SiO<sub>2</sub></b>		<b>C Blank + SiO<sub>2</sub> + Black dye</b>	
<b>Before</b>	<b>After</b>	<b>Before</b>	<b>After</b>	<b>Before</b>	<b>After</b>
0.021 ± 0.003	0.168 ± 0.086	0.141 ± 0.027	0.207 ± 0.079	0.214 ± 0.042	0.355 ± 0.125

		SEM	Si	Fe	Cr	Cu
Before	A					
	B					
	C					
After	A					
	B					
	C					



Nominal SiO <sub>2</sub> (wt%)	A Blank		B Blank + SiO <sub>2</sub>		C Blank + SiO <sub>2</sub> + Black dye	
	Before	After	Before	After	Before	After
SiO <sub>2</sub> on surface	72.41 ± 1.75	73.20 ± 1.75	75.40 ± 1.08	76.99 ± 1.49	62.78 ± 1.00	62.16 ± 1.42

**Table**

<b>T (°C)</b>	<b>A Blank</b>	<b>B Blank + SiO<sub>2</sub></b>	<b>C Blank + SiO<sub>2</sub> + Black dye</b>
<b>Troom</b> λ 5 – 20 μm	<b>0.892 ± 0.027</b>	<b>0.889 ± 0.027</b>	<b>0.890 ± 0.027</b>
<b>550 °C</b> λ 2 – 9 μm	<b>0.835 ± 0.029</b>	<b>0.838 ± 0.029</b>	<b>0.820 ± 0.029</b>